THE EUROPEAN PHYSICAL JOURNAL C

Chiral perturbation theory of the hyperfine splitting in (muonic) hydrogen

Franziska Hagelstein[1,2,3,a] ⓘ**, Vadim Lensky**[1]**, Vladimir Pascalutsa**[1]

[1] Institute of Nuclear Physics, Johannes Gutenberg Universität Mainz, 55099 Mainz, Germany
[2] PRISMA+ Cluster of Excellence, Johannes Gutenberg Universität Mainz, 55099 Mainz, Germany
[3] Laboratory for Particle Physics, Paul Scherrer Institute, 5232 Villigen PSI, Switzerland

Abstract The ongoing experimental efforts to measure the hyperfine transition in muonic hydrogen prompt an accurate evaluation of the proton-structure effects. At the leading order in α, which is $O(\alpha^5)$ in the hyperfine splitting (hfs), these effects are usually evaluated in a data-driven fashion, using the empirical information on the proton electromagnetic form factors and spin structure functions. Here we perform a first calculation based on the baryon chiral perturbation theory (BχPT). At leading orders it provides a prediction for the proton polarizability effects in hydrogen (H) and muonic hydrogen (μH). We find large cancellations among the various contributions leading to, within the uncertainties, a zero polarizability effect at leading order in the BχPT expansion. This result is in significant disagreement with the current data-driven evaluations. The small polarizability effect implies a smaller Zemach radius R_Z, if one uses the well-known experimental $1S$ hfs in H or the $2S$ hfs in μH. We, respectively, obtain $R_Z(\text{H}) = 1.010(9)$ fm, $R_Z(\mu\text{H}) = 1.040(33)$ fm. The total proton-structure effect to the hfs at $O(\alpha^5)$ is then consistent with previous evaluations; the discrepancy in the polarizability is compensated by the smaller Zemach radius. Our recommended value for the $1S$ hfs in μH is 182.640(18) meV.

Contents

1 Introduction

Muonic-atom spectroscopy has been successful at determining the charge radii of proton, deuteron, helion and alpha-particle with unprecedented precision through Lamb shift measurements [1–3]. It also holds the potential to impact tests of ab-initio nuclear theories and bound-state QED [4]. The proton Zemach radius R_Z has been extracted from a measurement of the $2S$ hyperfine splitting (hfs) in muonic hydrogen (μH) [5] with a 3.4% uncertainty:

$$R_Z(\mu\text{H}) = 1.082(37)\,\text{fm}, \tag{1}$$

by comparing to the theory prediction in Ref. [6] that relies on a data-driven evaluation of the proton polarizability contribution [7]:

$$E_{\text{hfs}}^{\text{pol.}}(2S, \mu\text{H}) = 8.0(2.6)\,\mu\text{eV}. \tag{2}$$

ᵃ e-mail: hagelste@uni-mainz.de (corresponding author)

Several collaborations are now preparing a measurement of the ground-state (1S) hfs in μH with ppm precision: CREMA [8], FAMU [9,10] and J-PARC [11] (see Ref. [12] for a comparison of the different experimental methods). These future measurements hold the potential to extract the Zemach radius with a sub-percent uncertainty, thereby constraining the magnetic properties of the proton.

A precise theory prediction for the 1S hfs in μH is essential for the success of the experimental campaigns. Firstly, to narrow down the frequency search range, which is important given the limited beam time available to the collaborations at PSI, RIKEN-RAL and J-PARC. Secondly, for the interpretation of the results. One can either extract the Zemach radius given a theory prediction for the proton-polarizability effect in the μH 1S hfs, or vice versa, extract the proton-polarizability effect with input for the Zemach radius. Furthermore, one can combine the precise measurements of the 1S hfs in H and μH to disentangle the Zemach radius and polarizability effects, leveraging radiative corrections as explained in Ref. [13], and compare their empirical values to theoretical expectations.

The biggest uncertainty in the theory prediction comes from proton-structure effects, entering through the two-photon exchange (TPE). These contain the above-mentioned Zemach radius and polarizability effects. Presently, they are evaluated within a "data-driven" dispersive approach [14–16]. While the dispersive method itself is rigorous, it requires sufficient experimental data to map out the proton spin structure functions $g_1(x, Q^2)$ and $g_2(x, Q^2)$ as full functions of the Bjorken variable x and the photon virtuality Q^2. This has been the aim of a dedicated "Spin Physics Program" at Jefferson Lab [17–21] that recently extended the previously scarce data for g_2 [22, 23].

In this work, we use an entirely different approach – the chiral perturbation theory (χPT) [24–26] – which has been successfully used to give a prediction for the proton-polarizability effect in the μH Lamb shift [27]. To be precise, we work in the framework of baryon chiral perturbation theory (BχPT) – the manifestly Lorentz-invariant formulation of χPT in the baryon sector [26,28,29] (see also [30,31] for reviews). We show that the leading-order (LO) BχPT prediction for the polarizability effect in the hfs is effectively vanishing, thereby, in substantial disagreement with the data-driven evaluations.

The paper is organized as follows. In Sect. 2, we discuss the forward TPE, and in particular, the polarizability effect in the hfs. A new formalism where one splits into contributions from the longitudinal-transverse and helicity-difference photoabsorption cross sections of the proton, σ_{LT} and σ_{TT}, is introduced in Eq. (12). It will be shown that

this decomposition is advantageous for both the dispersive, as well as the effective field theory (EFT) calculations as it gives a cleaner access to the uncertainties. More details are given in Appendix A. In Sect. 3, we present our LO BχPT prediction for the polarizability effect in the hfs of H and μH, together with a detailed discussion of the uncertainty estimate. In Sect. 4, we compare our results to data-driven dispersive and heavy baryon effective field theory (HB EFT) calculations. In Sect. 5, the Zemach radius is extracted from H and μH spectroscopy based on our prediction for the polarizability effect. In Sect. 6, we discuss the TPE effect in the μH hfs in view of the forthcoming experiments. Full details of the theoretical prediction for the 1S μH hfs are collected in Appendix C. We finish with an outlook and conclusions.

2 Two-photon exchange in the hyperfine splitting

The (muonic-)hydrogen hfs receives contributions from QED-, weak- and strong-interaction effects:

$$E_{\text{hfs}}(nS) = \frac{E_{\text{F}}}{n^3} \left(1 + \Delta_{\text{QED}} + \Delta_{\text{weak}} + \Delta_{\text{strong}} \right), \qquad (3)$$

where the leading-order in α contribution is given by the Fermi energy:

$$E_{\text{F}} = \frac{8Z\alpha}{3a^3} \frac{1 + \kappa}{mM}, \qquad (4)$$

with α the fine-structure constant, Z the charge of the nucleus (in the following $Z = 1$ for the proton), m, M the lepton and proton masses, κ the anomalous magnetic moment of the proton, and $a^{-1} = \alpha m_r$ the inverse Bohr radius, with $m_r = mM/(m + M)$ the reduced mass. The strong-interaction effects arise from the composite structure of the proton. They begin to enter at $\mathcal{O}(\alpha^5)$, see for instance Ref. [14], where they are split into the Zemach-radius, recoil, and polarizability contributions:

$$\Delta_{\text{strong}} = \Delta_{\text{Z}} + \Delta_{\text{recoil}} + \Delta_{\text{pol.}}, \qquad (5)$$

which can all be attributed to the forward TPE shown in Fig. 1. For a first comprehensive theory summary of the Lamb shift, fine and hyperfine structure in μH, including proton-structure dependent effects, we refer to Ref. [32]. The Zemach and recoil terms (Δ_{Z} and Δ_{recoil}) are elastic contributions with a proton in the intermediate state, see Fig. 1a. The diagram in Fig. 1b contains excited intermediate states (πN, Δ-isobar, etc.) represented by the 'blob'. It generates the polarizability effect ($\Delta_{\text{pol.}}$) that shall be evaluated in this work.

The forward TPE contribution to the hfs can be expressed through the spin-dependent forward doubly-virtual Compton scattering (VVCS) amplitudes, S_1 and S_2, cf. Eq. (A2). The latter can be related to the proton structure functions
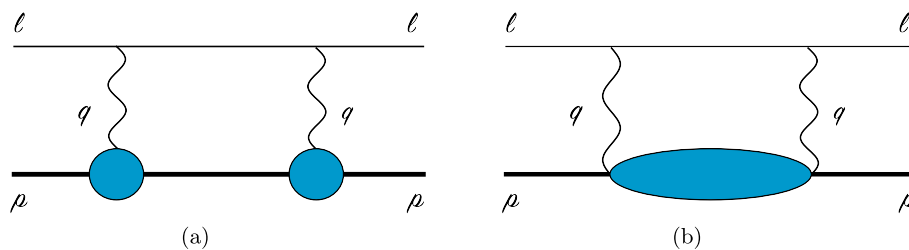
Fig. 1 Two-photon-exchange diagram in forward kinematics: **a** elastic contribution; **b** polarizability contribution. The horizontal lines correspond to the lepton and the proton (bold), where the 'blob' represents all possible excitations. The crossed diagrams are not drawn

g_1 and g_2 in a dispersive approach, cf. Eqs. (A12) and (A11). A full derivation of the well-known formalism for the TPE contribution to the hfs can be found in Appendix A.

The largest TPE effect is due to the Zemach radius contribution:

$$\Delta_Z = -2\alpha m_r R_Z. \tag{6}$$

The recoil contribution is one order of magnitude smaller [7], and will not be considered in this paper. It has been recently updated in Ref. [33]. The hfs is therefore best suited for a precision extraction of the Zemach radius, defined as the following integral over the electric and magnetic Sachs form factors $G_E(Q^2)$ and $G_M(Q^2)$ [32]:

$$R_Z = -\frac{4}{\pi} \int_0^\infty \frac{dQ}{Q^2} \left[\frac{G_E(Q^2)G_M(Q^2)}{1+\kappa} - 1 \right], \tag{7}$$

where $q^2 = -Q^2$ is the photon virtuality. Equivalently, we can write:

$$R_Z = \langle r \rangle_E + \langle r \rangle_M - \frac{2}{\pi^2} \int_0^\infty \frac{dt}{t} \frac{\mathrm{Im}\, G_M(t)}{1+\kappa}$$
$$\times \int_0^\infty \frac{dt'}{t'} \frac{\mathrm{Im}\, G_E(t')}{\sqrt{t} + \sqrt{t'}}, \tag{8}$$

where the linear electric and magnetic radii are defined as:

$$\langle r \rangle_{E,M} = \frac{2}{\pi} \int_0^\infty \frac{dt}{t^{3/2}} \,\mathrm{Im}\, G(t), \tag{9}$$

with $\mathrm{Im}\, G(t)$ the imaginary part of the normalized electric or magnetic Sachs form factor, $G_{E,M}(Q^2)/G_{E,M}(0)$. As one can see from Eqs. (7) and (8), a measurement of the Zemach radius gives access to the magnetic properties of the proton.

The polarizability effect in the hfs is fully constrained by empirical information on the proton spin structure functions $g_1(x, Q^2)$ and $g_2(x, Q^2)$, and the Pauli form factor $F_2(Q^2)$, functions of Q^2 and the Bjorken variable $x = Q^2/2M\nu$, where ν is the photon energy in the lab frame. This is in contrast to the Lamb shift, where the knowledge of a sub-

traction function, $T_1(0, Q^2)$ or $T_1(iQ, Q^2)$ [34], is needed.[1] It reads:[2]

$$\Delta_{\mathrm{pol.}} = \Delta_1 + \Delta_2 = \frac{\alpha m}{2\pi(1+\kappa)M} (\delta_1 + \delta_2), \tag{10a}$$

$$\delta_1 = 2 \int_0^\infty \frac{dQ}{Q} \left\{ \frac{5 + 4v_l}{(v_l + 1)^2} \left[4I_1(Q^2) + F_2^2(Q^2) \right] \right.$$
$$- \frac{32M^4}{Q^4} \int_0^{x_0} dx\, x^2 g_1(x, Q^2) \frac{1}{(v_l + v_x)(1 + v_x)(1 + v_l)}$$
$$\left. \times \left(4 + \frac{1}{1 + v_x} + \frac{1}{v_l + 1} \right) \right\}, \tag{10b}$$

$$\delta_2 = 96M^2 \int_0^\infty \frac{dQ}{Q^3} \int_0^{x_0} dx\, g_2(x, Q^2) \left(\frac{1}{v_l + v_x} - \frac{1}{v_l + 1} \right), \tag{10c}$$

with x_0 the inelastic threshold, $v_l = \sqrt{1 + 1/\tau_l}$, $v_x = \sqrt{1 + x^2\tau^{-1}}$, $\tau_l = Q^2/4m^2$, $\tau = Q^2/4M^2$, and the generalized Gerasimov–Drell–Hearn (GDH) integral:

$$I_1(Q^2) = \frac{2M^2}{Q^2} \int_0^{x_0} dx\, g_1(x, Q^2) = \bar{I}_1(Q^2) - F_2^2(Q^2)/4. \tag{11}$$

Here, $\bar{I}_1$ is the polarizability part of I_1. For the origin of the Pauli form factor in the above equations, see discussion in Appendix A.

As we will show in Sect. 3.2, instead of decomposing into Δ_1 and Δ_2, it is convenient to decompose into contributions from the longitudinal-transverse and helicity-difference cross sections σ_{LT} and σ_{TT}:

$$\Delta_{\mathrm{pol.}} = \Delta_{LT} + \Delta_{TT} + \Delta_{F_2}$$
$$= \frac{\alpha m}{2\pi(1+\kappa)M} \left(\delta_{LT} + \delta_{TT} + \delta_{F_2} \right), \tag{12a}$$

where we define:

$$\delta_{LT} = \frac{4M}{\alpha\pi^2} \int_0^\infty dQ \int_0^{x_0} dx\, \frac{1}{v_l + v_x} \frac{1}{x^2 + \tau}$$

---

[1] See Ref. [35] for a recent proposal how the subtraction functions can be related to integrals over photoabsorption cross sections.

[2] Note that our notation largely follows Ref. [36]. It differs slightly from other literature, where δ_i is usually denoted Δ_i [37].

$$\times \left[1 - \frac{1}{(1 + v_l)(1 + v_x)} \right] \sigma_{LT}(x, Q^2), \tag{12b}$$

$$\delta_{TT} = \frac{4M^2}{\alpha \pi^2} \int_0^\infty \frac{dQ}{Q} \int_0^{x_0} \frac{dx}{x} \frac{1}{1 + v_l}$$
$$\times \left[\frac{2\tau}{x^2 + \tau} + \frac{1}{(v_l + v_x)(1 + v_x)} \right] \sigma_{TT}(x, Q^2), \tag{12c}$$

$$\delta_{F_2} = 2 \int_0^\infty \frac{dQ}{Q} \frac{5 + 4v_l}{(v_l + 1)^2} F_2^2(Q^2). \tag{12d}$$

Or equivalently, in terms of the VVCS amplitudes, we can write:

$$\delta_{LT} = \frac{8M}{\alpha} \frac{1}{(2\pi)^3} \frac{1}{i} \int_{-\infty}^\infty dv \int d\mathbf{q} \frac{1}{Q^4 - 4m^2 v^2} \left\{ \bar{S}_1(v, Q^2) \right.$$
$$\left. + \frac{v}{M} \bar{S}_2(v, Q^2) \right\}$$
$$- \frac{4}{m^2} \int_0^\infty dQ \, Q \, (v_l - 1) F_2^2(Q^2), \tag{13a}$$

$$\delta_{TT} = \frac{4M}{\alpha} \frac{1}{(2\pi)^3} \frac{1}{i} \int_{-\infty}^\infty dv \int d\mathbf{q}$$
$$\times \frac{1}{Q^4 - 4m^2 v^2} \left\{ \frac{v}{M} \bar{S}_2(v, Q^2) - \frac{v^2}{Q^2} \bar{S}_1(v, Q^2) \right\}$$
$$- 2 \int_0^\infty \frac{dQ}{Q} \frac{1}{(v_l + 1)^2} F_2^2(Q^2). \tag{13b}$$

Here, $\bar{S}_i$ denotes the non-Born part of the amplitudes. An advantage of the BχPT calculation in this work is that the non-Born amplitudes can be calculated directly, and need not be constructed through the dispersive formalism. Furthermore, at the present order of our calculation in the BχPT power counting, there are no contributions to the elastic form factors, and thus, I_1 in Eq. (11) is given by the polarizability part only.

3 Chiral loops

Assuming BχPT is an adequate theory of low-energy nucleon structure, it should be well applicable to atomic systems, where the relevant energies are naturally small. In Ref. [27], the polarizability effect in the μH Lamb shift has been successfully predicted at LO in BχPT. Here, we extend this calculation to the polarizability effect in the hfs. This requires the spin-dependent non-Born VVCS amplitudes, $\bar{S}_1$ and $\bar{S}_2$, at chiral $\mathcal{O}(p^3)$ in the BχPT power counting.

Figure 1 in Ref. [27] shows the leading polarizability effect given by the TPE diagrams of elastic lepton-proton scattering with one-loop πN insertions. For the Compton-like processes, it is convenient to use the chirally-rotated leading BχPT Lagrangian for the pion $\pi^a(x)$ and nucleon $N(x)$

fields [38]:

$$\mathcal{L}_{\pi N}^{(1)} = \bar{N} \left(i \slashed{\partial} - M_N - i \frac{g_A}{f_\pi} M_N \tau^a \pi^a \gamma_5 + \frac{g_A^2}{2 f_\pi^2} M_N \pi^2 \right.$$
$$\left. + \frac{g_A^2 - 1}{4 f_\pi^2} \tau^a \epsilon^{abc} \pi^b \slashed{\partial} \pi^c \right) N + \mathcal{O}(\pi^3), \tag{14}$$

where $\gamma_5 = i \gamma^0 \gamma^1 \gamma^2 \gamma^3$, $g_A \simeq 1.27$ [39] is the axial coupling of the nucleon, $f_\pi \simeq 92.21$ MeV is the pion-decay constant, τ^a are the Pauli matrices, $M_N \simeq 938.27$ MeV and $m_\pi \simeq 139.57$ MeV are the nucleon and pion masses.[3] As described in Ref. [27], the Born part is separated from the $\mathcal{O}(p^3)$ VVCS amplitudes by subtracting the on-shell pion-loop γNN-vertex in the one-particle-reducible VVCS graphs, see diagrams (b) and (c) in Figure 1 of Ref. [27]. For more details on the BχPT framework, we refer to Refs. [40–42], where the complete next-to-next-to-leading-order (NNLO) in the δ-expansion [43] BχPT calculation of the spin-independent and spin-dependent nucleon VVCS amplitudes can be found.[4]

In practice, most results here were obtained based on our BχPT prediction for the πN-production channel in the structure functions g_i, given in Ref. [42, Appendix B]. It has been verified that the results agree with the calculation based on the VVCS amplitudes $\bar{S}_i$.

3.1 Numerical results

Our LO BχPT prediction for the polarizability effect in the $1S$ hfs of H and μH amounts to:

$$E_{hfs}^{\langle LO \rangle \, pol.}(1S, H) = 0.69(2.03) \, peV, \tag{15a}$$

$$E_{hfs}^{\langle LO \rangle \, pol.}(1S, \mu H) = 6.8(11.4) \, \mu eV. \tag{15b}$$

The error estimate will be described and motivated in the subsequent sections. The corresponding contributions to the nS hfs are trivially obtained through a $1/n^3$ scaling, as can be seen from Eqs. (3) and (4). Splitting into contributions from the spin structure functions g_1 and g_2, we obtain:

$$E_{hfs}^{\langle LO \rangle \, pol.}(1S, H, \Delta_1) = 0.3(3.1) \, peV,$$
$$E_{hfs}^{\langle LO \rangle \, pol.}(1S, H, \Delta_2) = 0.4(1.0) \, peV, \tag{16a}$$
$$E_{hfs}^{\langle LO \rangle \, pol.}(1S, \mu H, \Delta_1) = 5.2(16.5) \, \mu eV,$$
$$E_{hfs}^{\langle LO \rangle \, pol.}(1S, \mu H, \Delta_2) = 1.6(5.2) \, \mu eV. \tag{16b}$$

Strikingly, the contributions from the longitudinal-transverse and helicity-difference cross sections σ_{LT} and σ_{TT}:

$$E_{hfs}^{\langle LO \rangle \, pol.}(1S, H, \Delta_{LT}) = 5.1(1.5) \, peV,$$

---

[3] Note that isospin-breaking effects, such as differences in nucleon or pion masses, are neglected in the loops.

[4] See also Refs. [44–46] for nucleon VVCS studies in BχPT within the ϵ-expansion power-counting scheme [47].

$$E_{\text{hfs}}^{\langle \text{LO} \rangle \text{ pol.}}(1S, \text{H}, \Delta_{TT}) = -4.4(1.3) \, \text{peV}, \tag{16c}$$

$$E_{\text{hfs}}^{\langle \text{LO} \rangle \text{ pol.}}(1S, \mu\text{H}, \Delta_{LT}) = 30.0(9.0) \, \mu\text{eV},$$

$$E_{\text{hfs}}^{\langle \text{LO} \rangle \text{ pol.}}(1S, \mu\text{H}, \Delta_{TT}) = -23.2(7.0) \, \mu\text{eV}, \tag{16d}$$

are one order of magnitude larger than the total, and differ in their respective signs. This indicates a cancellation of LO contributions between Δ_{LT} and Δ_{TT}.

Including in addition the correction due to electron vacuum polarization (eVP) in the TPE diagram, see Fig. 10 and discussion in Appendix B, gives a negligible effect within the present uncertainties:

$$E_{\text{hfs}}^{\langle \text{LO} \rangle \text{ pol.} + \text{eVP}}(1S, \text{H}) = 0.72(2.07) \, \text{peV}, \tag{17a}$$

$$E_{\text{hfs}}^{\langle \text{LO} \rangle \text{ pol.} + \text{eVP}}(1S, \mu\text{H}) = 7.0(11.6) \, \mu\text{eV}. \tag{17b}$$

Nevertheless, it is important in view of the anticipated 1 ppm accuracy (corresponding to $\sim 0.2 \, \mu\text{eV}$) of the μH $1S$ hfs measurement by the CREMA collaboration [8]. We therefore include the additional $\Delta_{\text{pol.}}^{\text{eVP}}(\text{H}) = 0.01$ ppm and $\Delta_{\text{pol.}}^{\text{eVP}}(\mu\text{H}) = 1$ ppm on top of $\Delta_{\text{pol.}}(\text{H}) = 0.12(35)$ ppm and $\Delta_{\text{pol.}}(\mu\text{H}) = 37(62)$ ppm.

To understand why the contributions from σ_{LT} and σ_{TT} largely cancel in $\Delta_{\text{pol.}}$, we study the heavy-baryon (HB) limit of the spin-dependent VVCS amplitudes [48]. Expanding the LO BχPT expression for the $\bar{S}_1$ amplitude in $\mu = m_\pi/M_N$ while keeping the ratio of the light scales $\tau_\pi = Q^2/4m_\pi^2$ fixed, one obtains:

$$\bar{S}_1(0, Q^2) \overset{\text{HB}}{=} -\frac{3\alpha g_A^2}{16 f_\pi^2} m_\pi \left[1 - (1 + \tau_\pi) \frac{\arctan\sqrt{\tau_\pi}}{\sqrt{\tau_\pi}} \right]. \tag{18}$$

We then take a closer look at the first term in the low-energy polarizability expansion:

$$\frac{\bar{S}_1(0, Q^2)}{Q^2} \bigg|_{Q^2 \to 0} = M_N \left\{ \gamma_{E1M2} - 3\alpha M_N \left[P'^{(M1,M1)1}(0) \right. \right.$$
$$\left. \left. + P'^{(L1,L1)1}(0) \right] \right\}. \tag{19}$$

The HBχPT predictions for the proton polarizabilities [49–54] entering Eq. (19) read:

$$\gamma_{E1M2} = \frac{\alpha g_A^2}{(4\pi f_\pi)^2} \frac{1}{m_\pi^2} \frac{1}{6} \left[1 - \frac{7\pi}{4} \frac{m_\pi}{M_N} \right], \tag{20a}$$

$$P'^{(M1,M1)1}(0) = \frac{g_A^2}{(4\pi f_\pi)^2} \frac{1}{m_\pi^2} \frac{1}{18M} \left[-1 + \frac{7\pi}{4} \frac{m_\pi}{M_N} \right], \tag{20b}$$

$$P'^{(L1,L1)1}(0) = \frac{g_A^2}{(4\pi f_\pi)^2} \frac{1}{m_\pi^2} \frac{1}{9M} \left[1 - \frac{17\pi}{8} \frac{m_\pi}{M_N} \right]. \tag{20c}$$

We can see that the leading terms in the chiral expansion are of $\mathcal{O}(1/m_\pi^2)$. They cancel among the different polarizabili-

ties, thus, Eq. (21) becomes a subleading contribution:

$$\frac{\bar{S}_1(0, Q^2)}{Q^2} \bigg|_{Q^2 \to 0} \overset{\text{HB}}{=} \frac{\alpha g_A^2}{32 f_\pi^2} \frac{1}{m_\pi}. \tag{21}$$

Accordingly, one would expect the chiral loops in the hfs to be small. Indeed, the LO BχPT prediction in Eq. (15) is essentially vanishing, where the small number is mainly a remnant of higher orders in the HB expansion. This has to be taken into account in the uncertainty estimate.

Note that the HB expansion above has been introduced for instructive purposes only, but is not entering our calculation of the polarizability effect. The HBχPT prediction of the $S_1(0, Q^2)$ amplitude, Eq. (18), raises with Q, thus, its contribution to the hfs will be divergent. This can be seen from Fig. 2, where we compare the chiral-loop contribution to $\bar{S}_1(0, Q^2)$ as predicted by BχPT and HBχPT, respectively.

3.2 Uncertainty estimate

BχPT is a low-energy EFT of QCD describing strong interactions in terms of hadronic degrees of freedom (pion, nucleon, $\Delta(1232)$ resonance). An important requirement for a reliable BχPT prediction is that the contribution from beyond the scale at which this EFT is safely applicable, i.e., $Q_{\text{max}} > m_\rho = 775$ MeV, has to be small. For the LO BχPT prediction of the polarizability effect in the μH Lamb shift [27], the contribution from beyond this scale was less than 15%, thus, within the expected uncertainty. Comparing the TPE master formulas for Lamb shift and hfs, Eqs. (A8) and (A7), the weighting function in the former has a stronger suppression for large Q^2. It is therefore important to verify that the same quality criterion still holds for the hfs prediction presented here.

Let us consider the polarizability effect as a running integral with a momentum cutoff Q_{max}, as shown in Fig. 3. The convergence of the Δ_1 (green line) contribution, as well as

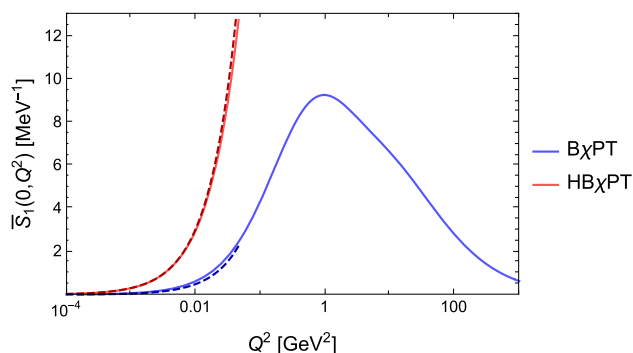**Fig. 2** The amplitude $\bar{S}_1(0, Q^2)$ at LO in BχPT (blue) and HBχPT (red). The dashed lines show the corresponding slope terms, i.e., the first terms in the expansion in powers of Q^2. The BχPT slope has been calculated from the polarizabilities given in Ref. [55, Table I], the HBχPT slope is given in Eq. (21)
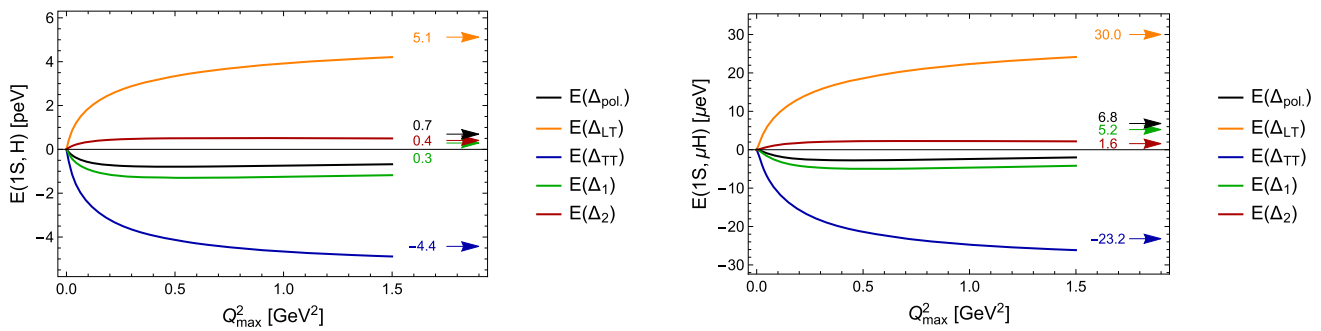
Fig. 3 Polarizability effect on the $1S$ hyperfine splitting in H (left panel) and μH (right panel): Cutoff dependence of the leading-order πN-loop contribution. The total results, Eqs. (15a) and (15b), are indicated by the black arrows

of the total $\Delta_{\text{pol.}}$ (black line), is poor. They display a sign change of the running integral at energies above $Q_{\max} \approx 2$ GeV (μH) and ≈ 4 GeV (H), respectively. Δ_2 (red line) converges better. Its contributions from above $Q_{\max} = m_\rho$ amount to 42% (H) and 26% (μH), respectively.

The bad high-momentum asymptotics indicated above are merely an artefact of the conventional splitting into Δ_1 and Δ_2. For the alternative splitting into Δ_{LT} and Δ_{TT}, introduced in Eq. (12), the cut-off dependence improves considerably. For Δ_{TT} (blue line), the contribution from above $Q_{\max} = m_\rho$ amounts to less than 4% for both hydrogens. For Δ_{LT} (orange line), the high-energy contributions are less than 35% (μH) and 32% (H), respectively. In this way, our results are in agreement with the natural expectation of uncertainty for a LO prediction, 30% [$\simeq (M_\Delta - M)/\text{GeV}$], in B$\chi$PT with inclusion of the Δ resonance. Based on this analysis, we decided to assign errors of 30% to the σ_{LT} and σ_{TT} contributions, and propagate them to Δ_1, Δ_2 and $\Delta_{\text{pol.}}$. It is interesting to note that in this way the uncertainty of Δ_1 is larger than the uncertainty of $\Delta_{\text{pol.}}$. This can be understood from the opposite signs of the $\Delta_{i,j}$ contributions, where $i = 1, 2$ and $j = LT, TT$, on the example of μH:

$$\Delta_{1,LT} = 227 \,\text{ppm}, \quad \Delta_{1,TT} = -198 \,\text{ppm}, \tag{22a}$$
$$\Delta_{2,LT} = -62 \,\text{ppm}, \quad \Delta_{2,TT} = 71 \,\text{ppm}. \tag{22b}$$

4 Comparison with other results

In this section, we compare our LO BχPT prediction for the polarizability effect in the H and μH hfs to other available evaluations. Furthermore, we study the contribution of the $\bar{S}_1(0, Q^2)$ subtraction function and the scaling of the polarizability effect with the lepton mass.

4.1 Heavy-baryon effective field theory

Let us start by comparing our BχPT prediction to other model-independent calculations using HB EFT [56–58].[5] First results for the elastic and inelastic TPE effects on the hfs in H and μH have been obtained in Ref. [56], where the contribution of the leading chiral logarithms, $\mathcal{O}(m^3 \alpha^5 / M^2 \times [\ln m_\pi, \ln \Delta, \ln m])$, was calculated in HB EFT matched to potential NRQED. At this order in the chiral expansion the polarizability effects in the hfs from pion-nucleon and pion-delta loops cancel each other in the large-N_c limit, while the Δ exchange cancels part of the point-like corrections, see also Ref. [48]. The analytical results presented in Refs. [56,59] motivate the relative size of the Zemach and polarizability corrections.

Updated HB EFT predictions for the TPE effects on the hydrogen spectra can be found in Refs. [57,58,60]. In Ref. [58], the difference between the pion-loop polarizability contributions in H and μH is quoted as

$$\Delta c_4 \equiv c_{4,\text{pol}}^{\mu\text{H}} - c_{4,\text{pol}}^{\text{H}} = 0.17(9), \tag{23}$$

where c_4 is a Wilson coefficient linked to the hfs in the following way:

$$E_{\text{hfs}}(nS) = \frac{E_{\text{F}}}{n^3} \frac{3\alpha}{2\pi(1+\kappa)} \frac{m}{M} c_4. \tag{24}$$

For comparison, we can evaluate the analogue of Δc_4 from other theory predictions for the polarizability contribution. Within errors, our LO BχPT prediction agrees with this result:

$$\Delta c_4 = 0.09(0.46). \tag{25}$$

Here, the uncertainties of the H and μH predictions have been combined in quadrature to estimate the error on their difference. For comparison, from the data-driven dispersive

---

[5] Full details on the BχPT framework used in here, and how it distinguishes from HB EFT, can be found in Ref. [27].
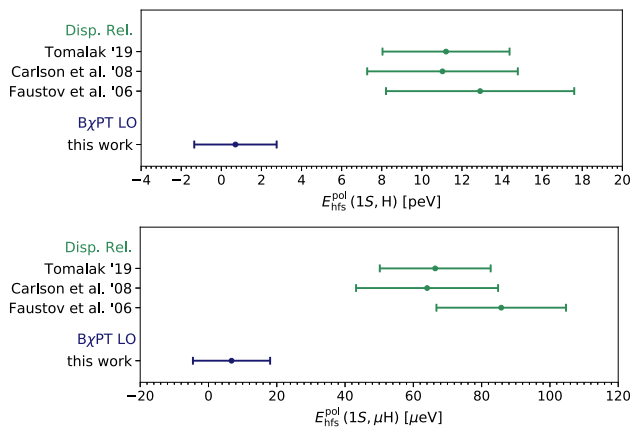
Fig. 4 Comparison of available results for the polarizability effect on the hyperfine splitting in H and μH (upper and lower panel) [14–16]

evaluations of Carlson et al. [14], one can deduce:

$$\Delta c_4 = -0.27(1.53), \tag{26}$$

where we combined all errors quoted in Ref. [14] and estimated the error on Δc_4 in the same way as done above.

4.2 Data-driven dispersive evaluations

There is a clear discrepancy between the BχPT prediction, presented here, and the conventional data-driven dispersive evaluations. The dispersive evaluations rely on empirical information for the inelastic proton spin structure functions, the elastic Pauli form factor and polarizabilities. The discrepancy can be seen from Fig. 4, where our LO BχPT prediction for the polarizability effect in the H and μH hfs is compared to the available dispersive evaluations. Adding an estimate for the next-to-leading-order (NLO) effect of the $\Delta(1232)$ resonance [61], obtained from large-N_c relations for the nucleon-to-delta transition form factors, to the model-independent LO BχPT prediction will improve agreement for Δ_2 but not for Δ_{pol}.

The origin of this discrepancy has to be understood in order to give a reliable prediction of the TPE effect in the μH hfs, needed for the forthcoming experiments. Part of the discrepancy might be due to underestimated uncertainties. An evaluation of the total polarizability effect suffers from cancellations in two places: firstly, between contributions from the cross sections σ_{LT} and σ_{TT}, secondly, between the elastic Pauli form factor F_2 and the inelastic structure functions in the low-Q region. Each of these cancellations reduces the result by an order of magnitude. In the calculation presented here, the former is taken into account by estimating the uncertainty due to higher-order corrections in the BχPT power counting based on the large σ_{LT} and σ_{TT} contributions, see discussion in Sect. 3.2. In the dispersive approach, it would be important to take into account corre-

lations between parametrizations of the g_1 and g_2 structure functions, which both rely on measurements of σ_{LT} and σ_{TT}. The latter cancellations in the low-Q region will be discussed in the following subsection.

4.3 Low-Q region and contribution of the $\bar{S}_1(0, Q^2)$ subtraction function

One major drawback of the data-driven dispersive evaluations is that they require independent input for the inelastic spin structure functions or related polarizabilities, and the elastic Pauli form factor. Our notation in Eq. (10b) conveniently illustrates how the zeroth moment of the inelastic spin structure function g_1 and the elastic Pauli form factor F_2 combine in the subtraction function:

$$\bar{S}_1(0, Q^2) = \frac{2\pi\alpha}{M} \left[F_2^2(Q^2) + 4I_1(Q^2) \right]$$
$$= \frac{8\pi\alpha}{M} \bar{I}_1(Q^2). \tag{27}$$

At $Q^2 = 0$, this is zero, because the Pauli form factor, $F_2(0) = \kappa$, and the generalized GDH integral, $I_1(0) = -\kappa^2/4$, so the two terms cancel exactly. A NLO BχPT prediction of the slope amounts to: $[\bar{I}_1]'(0) = 0.39(4)\,\text{GeV}^{-2}$ [42]. It can be expressed through a combination of lowest-order spin $[\gamma_{E1M2}]$ and generalized polarizabilities $[P'^{(M1,M1)1}(0)$ and $P'^{(L1,L1)1}(0)]$, see Eq. (19). In the HBχPT expansion, we showed that the leading $\mathcal{O}(1/m_\pi^2)$ terms cancel among these individual polarizabilities, given in Eq. (20), turning the result subleading in $\mathcal{O}(1/m_\pi)$, see Eq. (21). We can conclude that there is a strong cancellation between the elastic and inelastic contributions, which continues for higher Q^2.

The contribution of $\bar{S}_1(0, Q^2)$ to the hfs is given by:

$$E_{\text{hfs}}^{\langle \bar{S}_1(0,Q^2)\rangle}(nS) = \frac{E_{\text{F}}}{n^3} \frac{\alpha m}{\pi(1+\kappa)M} \int_0^\infty \frac{\text{d}Q}{Q} \frac{5+4v_l}{(v_l+1)^2}$$
$$\times \left[4I_1(Q^2) + F_2^2(Q^2) \right]. \tag{28}$$

Evaluations of this subtraction function contribution with empirical parametrizations for $g_1(x, Q^2)$ and $F_2(Q^2)$ tend towards larger values than the LO BχPT prediction. A partial calculation of the TPE effect at NLO in BχPT, considering only the one-loop box diagram with intermediate $\Delta(1232)$-excitation, will lower the theoretical prediction for the polarizability contribution from BχPT further, and in fact, turn it into a negative contribution [61,62]. Any imprecision in the empirical parametrizations, and thus in the cancellation between the elastic and inelastic moments, is enhanced by the $1/Q$ prefactor in the infrared region of the integral in Eq. (28). Therefore, the BχPT calculation, where the polarizability effect can be accessed directly through the non-Born part of the VVCS amplitudes and does not rely on input from separate measurements, has a clear advantage in this regard.

To illustrate this further, we reproduce the estimate for Δ_1 in the low-Q region from Ref. [14] (see references therein

for the details on the input). In this region, no experimental data from EG1 [63,64] exist and the integral is completed by interpolating data between higher Q^2 and $Q^2 = 0$, making use of empirical values for the static polarizabilities. For $Q^2 \in \{0, Q^2_{\max}\}$ with $Q^2_{\max} = 0.0452\,\text{GeV}^2$, the approximate formulas read [14]:

$$\delta_1(\text{H}) \sim \left(\underbrace{-\frac{3}{4}\kappa^2 r^2_{\text{Pauli}}}_{\to -2.19} + \underbrace{18M^2 c_{1B}}_{\to 3.54} \right) Q^2_{\max} = 1.35(90), \tag{29a}$$

$$\delta_1(\mu\text{H}) \sim \left[\underbrace{-\frac{1}{3}\kappa^2 r^2_{\text{Pauli}}}_{\to -1.45} + \underbrace{8M^2 c_1}_{\to 2.13} - \underbrace{\frac{M^2}{3\alpha}\gamma_0}_{\to 0.18} \right]$$
$$\times \int_0^{Q^2_{\max}} dQ^2 \beta_1(\tau_\mu) = 0.86(69), \tag{29b}$$

where

$$\beta_1(\tau_\mu) = -3\tau_\mu + 2\tau^2_\mu + 2(2 - \tau_\mu)\sqrt{\tau_\mu(\tau_\mu + 1)}. \tag{30}$$

Note that the formulas for H and μH differ, because one sets $m_e = 0$. The first terms are related to the elastic Pauli form factor, where $r_{\text{Pauli}} = -6/\kappa \, d/dQ^2 \, F_2(Q^2)|_{Q^2=0}$ is the Pauli radius. The other terms are related to the g_1 contribution. Considering the more general Eq. (29b), they are defined through:

$$I_1(Q^2) = M \int_{\nu_0}^\infty \frac{d\nu}{\nu^2} g_1(\nu, Q^2)$$
$$= -\kappa^2/4 + 2M^2 c_1 Q^2 + \mathcal{O}(Q^4), \tag{31a}$$

$$\gamma_0 = \frac{2\alpha}{M} \int_{\nu_0}^\infty \frac{d\nu}{\nu^4} g_1(\nu, 0). \tag{31b}$$

The strong cancellation between elastic and inelastic contributions, observed in Eq. (29), can be a source of uncertainty.

In addition, the quality of the low-Q approximation is rather poor. We can test it at LO in BχPT. Recall that at this order in the BχPT power counting, there is no contribution to the elastic form factors. Therefore, only the inelastic structure function g_1 enters. Our results are shown in Fig. 5. The approximate formulas in Eq. (29) give a 50% (67%) larger value for δ_1 in the region of $Q^2 < 0.0452\,\text{GeV}^2$ in the case of μH (H). Therefore, in the data-driven dispersive approach one has to properly account for the uncertainty introduced by the approximate formulas, as well as from cancellations between elastic and inelastic contributions.

4.4 Scaling with lepton mass

It is customary to use the high-precision measurement of the $1S$ hfs in H [65,66]:

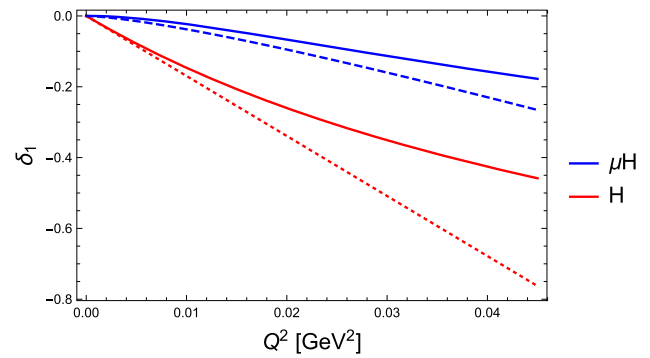$$E_{1S\text{-hfs}}^{\text{exp.}}(\text{H}) = 1\,420.405\,751\,768(1)\,\text{MHz}, \tag{32}$$

Fig. 5 The polarizability contribution δ_1 in the low-Q region for hydrogen (red) and muonic hydrogen (blue). The solid lines are the exact results according to Eq. (10b) with an upper cut on the Q integration. The dotted and dashed lines are evaluated with the approximate formulas for hydrogen and muonic hydrogen, respectively, see Eq. (29)

to refine the prediction of the TPE in the μH hfs [16,58] or the prediction of the total μH hfs [13]. We will do the same in Sect. 6. The strategies in Refs. [13,16,58] are slightly different, but all make statements about the scaling of various contributions to the hfs in a hydrogen-like atom when varying the lepton mass m_ℓ.

In Fig. 6, we study the scaling of the polarizability effect based on our LO BχPT prediction. In the left panel, we assume that the Δ_i (with $i = 1, 2, LT, TT$ and pol.) are scaling with the reduced mass m_r. In the right panel we assume that the δ_i are independent of the lepton mass, thus, Δ_i would be scaling with m_ℓ. The curves in the upper (lower) panel are normalized for H (μH), so they are fixed to 1 at $m_\ell = m_e$ ($m_\ell = m_\mu$). If the polarizability effect would scale according to our assumptions, i.e., $\propto m_r$ or $\propto m_\ell$, all curves would be constantly 1. We can see that the scaling works best for the contributions from σ_{LT} and σ_{TT}, which are large in their absolute values. Considering the total, in which the contributions from σ_{LT} and σ_{TT} cancel by about one order of magnitude, the scaling violation is enhanced by about one order of magnitude in relative terms. The same enhancement of the scaling violation can be observed for the numerically small contributions from g_1 and g_2. Comparing left and right panels, the BχPT predictions seem to support the assumption that Δ_{LT} and Δ_{TT} are scaling with m_r. For Δ_{LT}, the scaling is nearly perfect. For Δ_{TT}, we observe a violation of the scaling that is increasing with lepton mass. The approximation $\Delta_{TT}(\mu\text{H}) \sim m_r(\mu\text{H})/m_r(\text{H}) \, \Delta_{TT}(\mu\text{H})$ holds at the level of 10%. The approximation holds on a similar level after including an estimate for the NLO effect of the $\Delta(1232)$ resonance [61].

5 Extraction of the Zemach radius from spectroscopy

The TPE, entering the hfs, can be decomposed into Zemach radius, polarizability and recoil contributions, as described in Eq. (5). On top of the $\mathcal{O}(\alpha^5)$ TPE, we consider the lead-
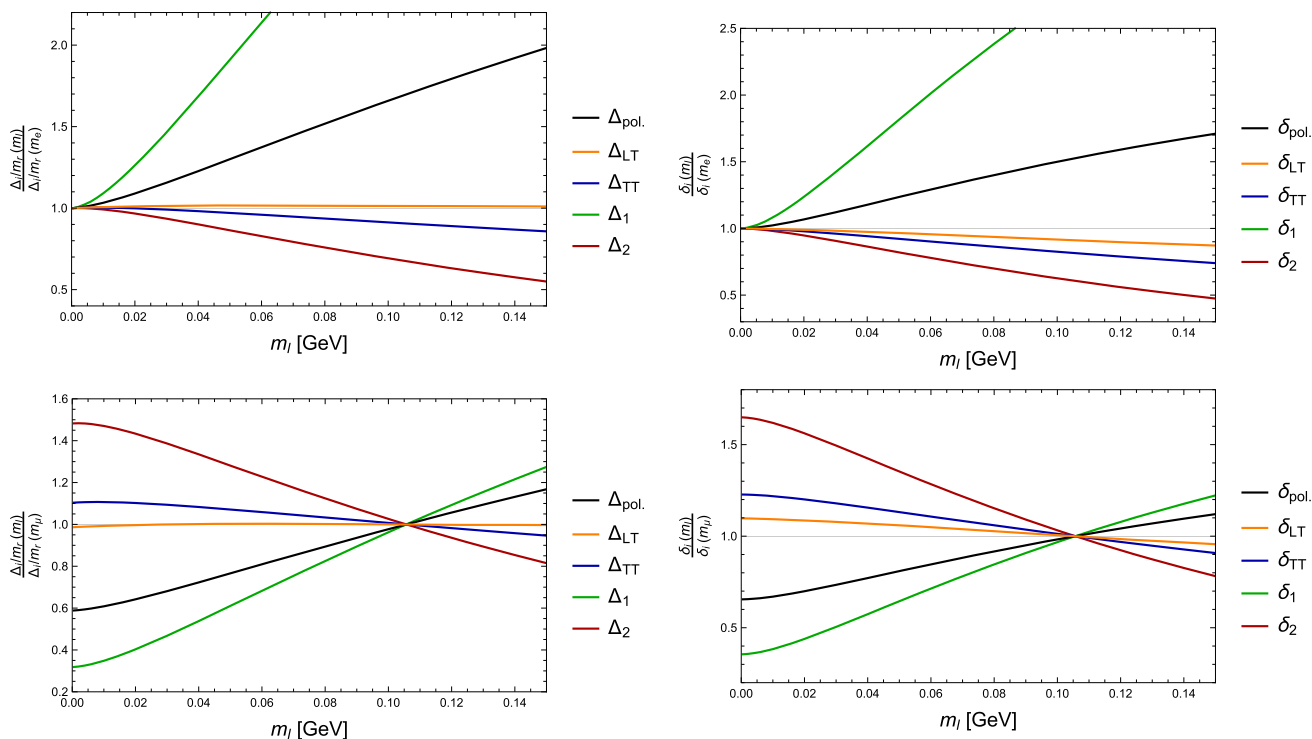
Fig. 6 Scaling of δ_i and Δ_i/m_r (with $i = 1, 2, LT, TT$ and pol.), as a function of the lepton mass m_ℓ

ing radiative corrections given by eVP, see Fig. 10 and discussion in Appendix B. Our prediction for the polarizability effect in the hfs, which is smaller than the conventional results from data-driven dispersive evaluations, also implies a smaller proton Zemach radius as previously determined from spectroscopy, cf. Eq. (1). In the following, we will extract the Zemach radius from the precisley measured $1S$ hfs in H, see Eq. (32), and the $2S$ hfs in μH [5]:

$$E_{\text{HFS}}^{\text{exp.}}(2S, \mu\text{H}) = 22.8089(51) \text{ meV}. \tag{33}$$

We use the theory predictions for the $1S$ hfs in H [13]:

up to a factor 3 more precise than the previous best determination [67] based on the electromagnetic form factors obtained from dispersion theory [68]. An itemized list of contributions to the $2S$ hfs in μH is given in Table 3 of Appendix C. From the LO BχPT prediction for the polarizability effect, including also the eVP in Eq. (17), we obtain:

$$R_{\text{Z}}(\text{H}) = 1.010(9) \text{ fm}, \tag{37a}$$

$$R_{\text{Z}}(\mu\text{H}) = 1.040(33) \text{ fm}. \tag{37b}$$

$$E_{\text{hfs}}(1S, \text{H}) = \left[1\,420\,453.106(10) \underbrace{-54.430(7)\left(\frac{R_{\text{Z}}}{\text{fm}}\right) + E_{\text{F}}\left(0.99807(13)\,\Delta_{\text{recoil}} + 1.00002\,\Delta_{\text{pol.}}\right)}_{\text{TPE including radiative corrections}} \right] \text{kHz} \tag{34}$$

and the $2S$ hfs in μH [13]:

$$E_{\text{hfs}}(2S, \mu\text{H}) = \left[22.9584(8) \underbrace{-0.16319(2)\left(\frac{R_{\text{Z}}}{\text{fm}}\right) + \frac{E_{\text{F}}}{8}\left(1.01580(4)\,\Delta_{\text{recoil}} + 1.00326\,\Delta_{\text{pol.}}\right)}_{\text{TPE including radiative corrections}} \right] \text{meV}, \tag{35}$$

with the recently re-evaluated $\mathcal{O}(\alpha^5)$ recoil correction [33]:

$$\Delta_{\text{recoil}}(\text{H}) = 5.269\,^{+0.017}_{-0.004} \text{ ppm}, \tag{36a}$$

$$\Delta_{\text{recoil}}(\mu\text{H}) = 837.6\,^{+2.8}_{-1.0} \text{ ppm}, \tag{36b}$$

Table 1 Determinations of the proton Zemach radius R_Z, in units of fm

ep scattering		μH 2S hfs		H 1S hfs	
Lin et al. '21 [68]	Borah et al. '20 [69]	Antognini et al. '13 [5]	LO BχPT	Volotka et al. '04 [75]	LO BχPT
$1.054^{+0.003}_{-0.002}$	1.0227(107)	1.082(37)	1.040(33)	1.045(16)	1.010(9)
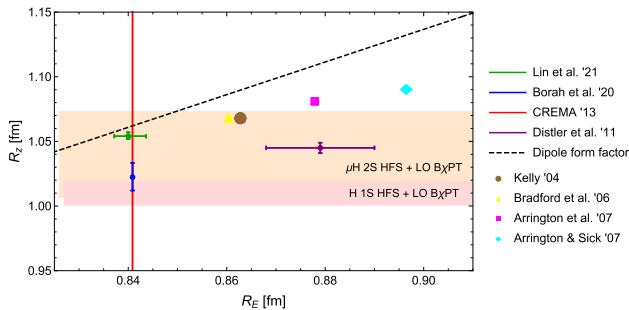
Fig. 7 Correlation between the Zemach and charge radius of the proton. Our extractions based on LO BχPT are compared to results from Lin et al. [68], Borah et al. [69], CREMA [5], Distler et al. [70], Kelly [71], Bradford et al. [72], Arrington et al. [73], and Arrington and Sick [74]

This can be compared to other determinations of the proton Zemach radius collected in Table 1.[6] The radii we find are in agreement with the proton form factor analysis from Ref. [69], which uses the proton charge radius from the μH Lamb shift [5] as a constraint for their fit.

Figure 7 shows how the Zemach and charge radius of the proton are correlated. It suggests that a "smaller" charge

radius, as seen initially in the μH Lamb shift by the CREMA collaboration [5] (red line), comes with a "smaller" Zemach radius. The dashed black curve is calculated with a dipole form, $G(Q^2) \propto (1 + Q^2/\Lambda^2)^{-2}$, for the electric and magnetic Sachs form factors, by varying Λ. The light red and orange bands show R_Z as extracted by us, Eq. (37), based on the LO BχPT prediction for the polarizability effect in the hfs.

6 Theory prediction for the ground-state hyperfine splitting in μH

The upcoming measurements of the 1S hfs in μH [8–11] crucially rely on a precise theory prediction. The limiting uncer-

Fig. 8 Two-photon-exchange effect on the 1S hyperfine splitting in μH [14, 16, 58]
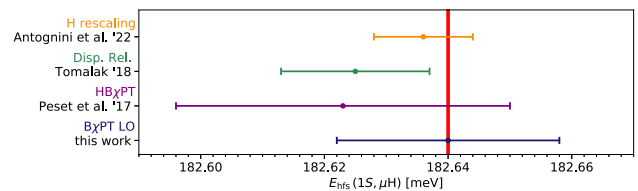
Fig. 9 Predictions for the 1S hyperfine splitting in μH [13, 16, 58], compared to the *projected uncertainty* of the planned CREMA measurement (red vertical line)

tainty is given by the TPE, which is conventionally split into Zemach radius, polarizability and recoil contributions [13]:

$$E_{\text{hfs}}(1S, \mu H) = \left[183.797(7) \underbrace{- 1.30653(17) \left(\frac{R_Z}{\text{fm}} \right) + E_F \left(1.01656(4) \, \Delta_{\text{recoil}} + 1.00402 \, \Delta_{\text{pol.}} \right)}_{\text{TPE including radiative corrections}} \right] \text{meV}, \tag{38}$$

see Appendix C and Table 2 for an itemized list of the individual contributions. As explained in Sect. 4.4, it is customary to refine the theory prediction of 1S hfs in μH with the help of the high-precision measurement of the 1S hfs in H. We do so by combining our BχPT prediction for the polarizability effect in the μH hfs, Eq. (17b), and the Zemach radius extracted from H spectroscopy, Eq. (37a), based on the same prediction for the polarizability effect in the H hfs. We arrive at:

$$E_{\text{hfs}}(1S, \mu H) = 182.640(18) \text{ meV}, \tag{39a}$$
$$E_{\text{hfs}}^{\text{TPE}}(1S, \mu H) = -1.157(16) \text{ meV}, \tag{39b}$$

where $E_{\text{hfs}}^{\text{TPE}}$ corresponds to the TPE including radiative corrections and recoil corrections from Ref. [33], as indicated by the curly brace in Eq. (38).

In Figs. 8 and 9, we compare our predictions to results from data-driven dispersive evaluations [14, 16] and HB EFT [58]. While almost all available predictions for the total hfs in μH are in agreement after the H refinement procedure, further

---

[6] Note that the chiral logarithm result for the Zemach radius [57], $R_Z = 1.35$ fm, is substantially larger than all extractions from experiment.
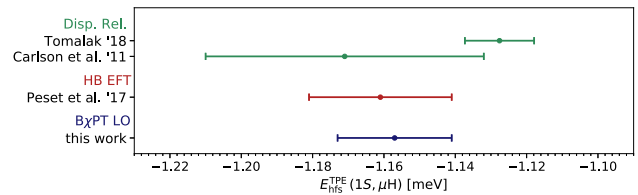
improvements of the theory are required in order to compete with the anticipated experimental accuracy.

7 Conclusions and outlook

We have presented the LO BχPT prediction for the $\mathcal{O}(\alpha^5)$ polarizability effect on the hfs in H and μH, see Eq. (15). Contrary to the data-driven evaluations, the BχPT prediction is compatible with zero. This was expected from the HBχPT limit of the VVCS amplitudes, in particular $\bar{S}_1(0, Q^2)$, which partially display a cancellation of the leading order in the chiral expansion of small m_π, see discussion in Sect. 3.1. The small polarizability effect is then mainly a remnant of higher orders in the HB expansion.

A new formalism where the polarizability effect is split into contributions from the longitudinal-transverse and helicity-difference cross sections, σ_{LT} and σ_{TT}, instead of contributions from the spin structure functions, g_1 and g_2, has been introduced in Eq. (12). It was shown that these contributions, Δ_{LT} and Δ_{TT}, cancel by one order of magnitude when combined into $\Delta_{\text{pol.}}$. Only Δ_{LT} and Δ_{TT} are good observables in the BχPT framework, for which the contributions from beyond the scale at which this EFT is safely applicable, $Q_{\max} > m_\rho = 775$ MeV, are within the expected uncertainty. In addition, only Δ_{LT} and Δ_{TT} satisfy the conventionally assumed scaling with the reduced mass m_r of the hydrogen-like system to 10% relative accuracy, while the cancellations in $\Delta_{\text{pol.}}$ enhance any violation in the scaling by one order of magnitude.

As shown in Fig. 4, our model-independent LO BχPT prediction is substantially smaller than the data-driven dispersive evaluations. An estimate for the effect of the $\Delta(1232)$-resonance [61], obtained from large-N_c relations for the nucleon-to-delta transition form factors, shows that the discrepancy is likely to increase at the NLO. The smaller polarizability effect, in turn, leads to a smaller Zemach radius as extracted from the experimental 1S hfs in H and the 2S hfs in μH, cf. Eq. (37). Therefore, resolving the present discrepancy for the polarizability effect is crucial for the analysis of the forthcoming measurements of the 1S hfs in μH and the extraction of the Zemach radius.

The data-driven approach relies on empirical information on the inelastic spin structure functions, or the measured cross sections to be precise, as well as the elastic form factors and polarizabilities at $Q^2 = 0$. Due to the large cancellations between σ_{LT} and σ_{TT}, as well as g_1 and F_2, precise parametrizations of the former are needed, and the uncertainty of the TPE evaluation has to be estimated with great care, taking into account all correlations. Furthermore, due to a lack of data at low Q, one uses interpolation from $Q^2 = 0$ to the onset of data [14]. As we showed in Sect. 4.3 based on LO BχPT, the quality of these approximations is rather

poor and is yet another source of uncertainty. New data from the Jefferson Lab "Spin Physics Program" [17–21], including also the substantially extended dataset for g_2 [23], will allow for a re-evaluation of the polarizability effect on the hfs in H and μH.

An accurate theoretical prediction of the 1S hfs in μH is crucial for the future measurement campaigns, since it allows to reduce the search range for the resonance in experiment. Thus, one might find the resonance faster and acquire more statistics during the allocated beam time, see discussion in Ref. [13]. The present discrepancy between predictions for the polarizability effect can be mended, if the high-precision measurement of the 1S hfs in H is implemented as a constraint. Applying this procedure, good agreement is found between all theory predictions for the total 1S hfs in μH hfs, see Fig. 9. Eventually, after a successful measurement of the 1S hfs in μH, one can combine it with the 1S hfs in H to disentangle the Zemach radius and polarizability effects, leveraging radiative corrections as explained in Ref. [13]. The empirical polarizability effect, obtained in this way, can reach a precision of ~ 40 ppm [13]. That is sufficient to discriminate between the presently inconsistent theoretical predictions.

Data availability statement This manuscript has no associated data or the data will not be deposited. [Authors' comment: All data relevant to this study are included in the article or can be obtained from the sources referenced therein.]

Appendix A: Two-photon-exchange master formula and dispersive approach

The proton-structure effects at $\mathcal{O}(\alpha^5)$ are described by TPE in forward kinematics, i.e., by the diagram in Fig. 1 where the momentum transfer between the initial and final particles is vanishing. The (forward) TPE can be related to the amplitudes of (forward) VVCS off the proton, which in turn can be expressed in terms of proton structure functions via dispersion relations. A detailed review of the VVCS theory can be found in Ref. [36, Section 5]. Even though the TPE formalism is well-known, see for instance Ref. [7,14], we will present here its derivation for the hfs.[7]

As implied above, it is customary to split the TPE into leptonic and hadronic tensors ($L^{\mu\nu}$ and $T^{\mu\nu}$):

$$
\mathcal{M} = \frac{1}{2} \int \frac{\mathrm{d}^4 q}{i (2\pi)^4} \frac{1}{q^4} \left[\bar{u}(\ell) L_{\mu\nu}(\ell, q) u(\ell) \right] \\
\times \left[\bar{N}(p) T^{\mu\nu}(p, q) N(p) \right], \tag{A1}
$$

where $u(\ell)$ and $N(p)$ are the lepton and proton Dirac spinors, with ℓ, p and q being the lepton, proton and photon four-momenta (see Fig. 1), respectively. Here, a factor of $1/2$ has been introduced to avoid double counting when contracting the crossing-invariant tensors.

Only the spin-dependent part of the forward VVCS will contribute to the hfs. For the proton, it reads:[8]

$$
T_A^{\mu\nu}(q, p) = -\frac{1}{M} \gamma^{\mu\nu\alpha} q_\alpha \, S_1(\nu, Q^2) + \frac{Q^2}{M^2} \gamma^{\mu\nu} S_2(\nu, Q^2), \tag{A2}
$$

where S_1 and S_2 are two independent scalar functions of the photon lab-frame energy ν and the photon virtuality $Q^2 = -q^2 = \mathbf{q}^2 - \nu^2$. Equivalently, one can write Eq. (A2) with the help of the spin four-vector s^α (satisfying $\mathsf{s}^2 = -1$ and $\mathsf{s} \cdot p = 0$):[9]

$$
T_A^{\mu\nu}(q, p) = \frac{i}{M} \epsilon^{\mu\nu\alpha\beta} q_\alpha \mathsf{s}_\beta \, S_1(\nu, Q^2) + \frac{i}{M^3} \epsilon^{\mu\nu\alpha\beta} \\
\times q_\alpha (p \cdot q \, \mathsf{s}_\beta - \mathsf{s} \cdot q \, p_\beta) S_2(\nu, Q^2). \tag{A3}
$$

Since $T_A^{\mu\nu}$ is antisymmetric in its indices, it is sufficient to replace the lepton tensor with the antisymmetric part of the tree-level QED amplitude of forward VVCS [in the structureless limit with the Dirac and Pauli form factors $F_1 \to 1$

and $F_2 \to 0$, cf. Eqs. (A2) and (A10)]:[10]

$$
L_A^{\mu\nu} = \frac{-2\pi\alpha \, Q^2}{(\ell \cdot q)^2 - \frac{1}{4} Q^4} \gamma^{\mu\nu\alpha} q_\alpha. \tag{A4}
$$

The lepton and proton momenta are of typical atomic scales, thus, much smaller than the other scales we are considering. Therefore, in the center-of-mass frame, we assume both of them to be at rest, $p = M/m \, \ell = (M, \mathbf{0})$:[11]

$$
\left[\bar{u}(\ell) \gamma_{\mu\nu\alpha} q^\alpha u(\ell) \right] \left[\bar{N}(p) \gamma^{\mu\nu} N(p) \right] = 8\nu \, s \cdot S, \\
\left[\bar{u}(\ell) \gamma_{\mu\nu\alpha} q^\alpha u(\ell) \right] \left[\bar{N}(p) \gamma^{\mu\nu\beta} q_\beta N(p) \right] = \frac{8}{3} (\nu^2 - 2Q^2) \, s \cdot S, \tag{A5}
$$

with the lepton and proton spin operators s and S, and $\ell \cdot q = m\nu$.

The forward TPE generates a $\delta(\mathbf{r})$-function potential: $V(r) = \mathcal{M} \, \delta(\mathbf{r})$. Treated in perturbation theory, such kind of potential generates an energy shift of the nS levels: $E_{nS} = \phi_n^2 \mathcal{M}$, where $\phi_n^2 = 1/(\pi a^3 n^3)$ is the hydrogen wave function at the origin. When acting on the wave functions, the product of spin operators can be replaced by the atom's total angular momentum f [76]:

$$
s \cdot S \xrightarrow{nS \text{ level}} \frac{1}{2} \left[f(f+1) - \frac{3}{2} \right]. \tag{A6}
$$

Recalling that the nS hfs is defined as the splitting between S levels with $f = 1$ and $f = 0$, we finally arrive at the following master formula for the TPE contribution to the hfs in terms of proton VVCS amplitudes:

$$
E_{\text{hfs}}^{\text{TPE}}(nS) = \frac{E_{\text{F}}}{n^3} \frac{4m}{1+\kappa} \frac{1}{i} \int_{-\infty}^\infty \frac{\mathrm{d}\nu}{2\pi} \int \frac{\mathrm{d}\mathbf{q}}{(2\pi)^3} \frac{1}{Q^4 - 4m^2\nu^2} \\
\times \left\{ \frac{(2Q^2 - \nu^2)}{Q^2} S_1(\nu, Q^2) + \frac{3\nu}{M} S_2(\nu, Q^2) \right\}. \tag{A7}
$$

The Lamb shift analogue reads:

$$
E_{nS}^{\text{TPE}} = 8\pi\alpha m \, \phi_n^2 \frac{1}{i} \int_{-\infty}^\infty \frac{\mathrm{d}\nu}{2\pi} \int \frac{\mathrm{d}\mathbf{q}}{(2\pi)^3} \\
\times \frac{(Q^2 - 2\nu^2) T_1(\nu, Q^2) - (Q^2 + \nu^2) T_2(\nu, Q^2)}{Q^4 (Q^4 - 4m^2\nu^2)}, \tag{A8}
$$

---

[7] An extensive discussion of the TPE formalism, considering in addition the Lamb shift, can also be found in Ref. [62, Chapter 5].

[8] We define $\gamma_{\mu\nu} = \frac{1}{2} [\gamma_\mu, \gamma_\nu]$ and $\gamma_{\mu\nu\alpha} = \frac{1}{2} (\gamma_\mu \gamma_\nu \gamma_\alpha - \gamma_\alpha \gamma_\nu \gamma_\mu)$.

[9] The symmetric spin-independent part of forward VVCS reads:

$$
T_S^{\mu\nu}(q, p) = -g^{\mu\nu} T_1(\nu, Q^2) + \frac{p^\mu p^\nu}{M^2} T_2(\nu, Q^2),
$$

where terms vanishing upon contraction with the lepton tensor are not shown.

[10] The symmetric part of the tree-level QED amplitude of forward VVCS, contributing to the Lamb shift, reads:

$$
L_S^{\mu\nu} = \frac{4\pi\alpha}{m} \frac{1}{(\ell \cdot q)^2 - \frac{1}{4} Q^4} \\
\times \left[g^{\mu\nu} (\ell \cdot q)^2 - (q^\mu \ell^\nu + q^\nu \ell^\mu) \ell \cdot q - Q^2 l^\mu l^\nu \right].
$$

[11] Averaging over the angles of q gives $(q \cdot s)(q \cdot S) \to 1/3 \, q^2 (s \cdot S)$ and so on for other combinations.

where T_1 and T_2 are the spin-independent forward VVCS amplitudes.

The VVCS amplitudes can be split into Born and non-Born parts:

$$S_1(\nu, Q^2) = S_1^{\text{Born}}(\nu, Q^2) + \bar{S}_1(\nu, Q^2), \tag{A9a}$$

$$S_2(\nu, Q^2) = S_2^{\text{Born}}(\nu, Q^2) + \bar{S}_2(\nu, Q^2), \tag{A9b}$$

where Born corresponds to the simplest tree-level diagrams with a proton in the intermediate state, and non-Born corresponds to everything else. The finite-size recoil and Zemach radius effects are described by the well-known Born part of the VVCS amplitudes [77]:

$$
\begin{aligned}
&S_1^{\text{Born}}(\nu, Q^2) \\
&= \frac{2\pi\alpha}{M}\left[\frac{4M^2 Q^2\, G_M(Q^2) F_1(Q^2)}{Q^4 - 4M^2\nu^2} - F_2^2(Q^2)\right],
\end{aligned}
\tag{A10a}
$$

$$S_2^{\text{Born}}(\nu, Q^2) = -\frac{8\pi\alpha M^2 \nu}{Q^4 - 4M^2\nu^2}\, G_M(Q^2) F_2(Q^2), \tag{A10b}$$

where $F_1(Q^2)$ and $F_2(Q^2)$ are the Dirac and Pauli form factors of the proton, and $G_M(Q^2) = F_1(Q^2) + F_2(Q^2)$ is the magnetic Sachs form factor. The Zemach radius and its effect on the hfs are defined in Eqs. (6) and (7). Exact formulas for the TPE recoil contribution can be found for instance in Ref. [7]. The polarizability effect is described by the non-Born part of the VVCS amplitudes.

Using the general principles of analyticity, unitarity, crossing symmetry and gauge invariance, one can conveniently express the spin-dependent VVCS amplitudes through the proton spin structure functions $g_1(x, Q^2)$ and $g_2(x, Q^2)$ by means of the optical theorem:

$$
\begin{aligned}
\text{Im}\, S_1(\nu, Q^2) &= \frac{4\pi^2\alpha}{\nu}\, g_1(x, Q^2) \\
&= \frac{M\nu^2}{\nu^2 + Q^2}\left[\frac{Q}{\nu}\sigma_{LT} + \sigma_{TT}\right](\nu, Q^2),
\end{aligned}
\tag{A11a}
$$

$$
\begin{aligned}
\text{Im}\, S_2(\nu, Q^2) &= \frac{4\pi^2\alpha M}{\nu^2}\, g_2(x, Q^2) \\
&= \frac{M^2\nu}{\nu^2 + Q^2}\left[\frac{\nu}{Q}\sigma_{LT} - \sigma_{TT}\right](\nu, Q^2),
\end{aligned}
\tag{A11b}
$$

and dispersion relations:

$$
\begin{aligned}
\bar{S}_1(\nu, Q^2) &= \frac{2\pi\alpha}{M}\left\{\left[F_2^2(Q^2) + 4I_1(Q^2)\right] + \frac{32M^4\nu^2}{Q^6}\right. \\
&\quad \left. \times \int_0^{x_0} dx\, \frac{x^2 g_1(x, Q^2)}{1 - x^2(\nu/\nu_{\text{el}})^2 - i0^+}\right\},
\end{aligned}
\tag{A12a}
$$

$$
\begin{aligned}
\nu\bar{S}_2(\nu, Q^2) &= \frac{64\pi\alpha M^4\nu^2}{Q^6} \\
&\quad \times \int_0^{x_0} dx\, \frac{x^2 g_2(x, Q^2)}{1 - x^2(\nu/\nu_{\text{el}})^2 - i0^+},
\end{aligned}
\tag{A12b}
$$

with $\nu_{\text{el}} = Q^2/2M$ and $I_1(Q^2)$ defined in Eq. (11). As shown in Eq. (A11), the spin structure functions correspond to certain combinations of photoabsorption cross sections. Here, σ_{LT} is the longitudinal-transverse photoabsorption cross section describing a spin-flip of the proton, and $\sigma_{TT} = 1/2\,(\sigma_{1/2} - \sigma_{3/2})$ is the helicity-difference cross section for transversely polarized photons, where the subscripts on $\sigma_{1/2}$ and $\sigma_{3/2}$ denote the total helicity of the $\gamma^* N$ state.

To solve Eq. (A7) one uses a Wick rotation to imaginary energies, and hyperspherical coordinates. Employing the dispersive representation from Eq. (A12), after the angular integrations one obtains the polarizability effect as presented in Eq. (10), where one conventionally splits into contributions from g_1 and g_2. As we explain in our paper, in view of the uncertainty estimate, it is favorable to consider instead a splitting into contributions from σ_{LT} and σ_{TT}, derived by us in Eq. (12).

It is worth to discuss some subtleties entering the definition of the polarizability effect through the non-Born VVCS amplitudes in the dispersive approach. Naively, one would expect the Born and non-Born amplitudes to be expressed entirely through elastic form factors and inelastic structure functions, respectively. Instead, one finds:

$$
\begin{aligned}
&S_1^{\text{elastic}}(\nu, Q^2) - S_1^{\text{Born}}(\nu, Q^2) \\
&= \bar{S}_1(\nu, Q^2) - S_1^{\text{inelastic}}(\nu, Q^2) = \frac{2\pi\alpha}{M} F_2^2(Q^2),
\end{aligned}
\tag{A13a}
$$

$$
\begin{aligned}
&[\nu S_2]^{\text{elastic}}(\nu, Q^2) - \nu S_2^{\text{Born}}(\nu, Q^2) \\
&= \nu\bar{S}_2(\nu, Q^2) - [\nu S_2]^{\text{inelastic}}(\nu, Q^2) \\
&= -2\pi\alpha\, F_2(Q^2) G_M(Q^2),
\end{aligned}
\tag{A13b}
$$

where S_1^{elastic} and $[\nu S_2]^{\text{elastic}}$ are pure nucleon-pole terms. In Eq. (A12a), the necessary conversion term to obtain the non-Born amplitude, given on the right-hand side of Eq. (A13a), is easily seen. Here, even though S_1 satisfies an unsubtracted dispersion relation, we wrote a once-subtracted dispersion relation, with the subtraction term $\bar{S}_1(0, Q^2)$ defined in Eq. (27). This is useful to emphasize the interplay of the elastic Pauli form factor F_2 and the inelastic spin structure function g_1, as explained in Sects. 2 and 4.3. For Eq. (A12b), the applied conversion procedure is less obvious. Starting from a dispersion relation for νS_2:[12]

$$\nu S_2(\nu, Q^2) = 2\pi\alpha\,\frac{2}{\tau}\int_0^1 dx\, \frac{g_2(x, Q^2)}{1 - x^2(\nu/\nu_{\text{el}})^2 - i0^+},$$

---

[12] The amplitude S_2 does have a pole in the subsequent limit of $Q^2 \to 0$ and $\nu \to 0$.

Table 2 $1S$ hfs in μH. All values in meV

	Contribution	Our Choice	References
h1	Fermi energy, $(Z\alpha)^4$	182.44333	
h2	Breit corr., $(Z\alpha)^6$	0.01457	
h4	μ anomalous magnetic moment corr., $\alpha(Z\alpha)^4$	0.21271	
h5	eVP in 2nd-order PT, $\alpha^2(Z\alpha)^4 m_r$	0.73449	[79, Table 1 b)]
h7	Two-loop corr. to Fermi energy, $\alpha^2(Z\alpha)^4 m_r$	0.00556	[79, Table 2 c) and d)]
h8	One-loop eVP in 1γ int., $\alpha(Z\alpha)^4 m_r$	0.37465	[79, Table 1 a)]
h9	Two-loop eVP in 1γ int., $\alpha^2(Z\alpha)^4 m_r$	0.00292	[79, Table 2 a) and b)]
h10	Further two-loop eVP corr. in 2nd and 3rd-order PT	0.00387	[79, Table 2 e), f) and g)]
h11	μVP	0.00729	$\sim E_F\,\alpha(Z\alpha)\,3/4$
h13	Vertex, $\alpha(Z\alpha)^5$	-0.02484	$\sim E_F\,\alpha(Z\alpha)\,[\ln 2 - 13/4]$
h14	Higher-order corr. $\alpha(Z\alpha)^6$	-0.00128	[80, Eq. 7.1]
h18	hVP, α^6	0.00356	[81]
h19	Weak interaction contribution	0.00221	[82, Eq. 374]
h28	Recoil corr. with p AMM, α^6	0.01752	[14, Eq. 22] and [83]
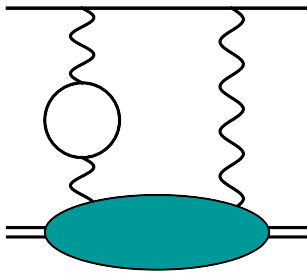
Fig. 10 Two-photon exchange with vacuum-polarization insertion at $O(\alpha^6)$.

$$(A14)$$

we separate the inelastic part (i.e., limit the integration to $x \in \{0, x_0\}$) and add the conversion term from the right-hand side of Eq. (A13b). The latter then cancels the inelastic part of the zeroth moment of the g_2 structure function, due to the Burkhardt–Cottingham (BC) sum rule [78]:

$$0 = \int_0^1 \mathrm{d}x\, g_2(x,\, Q^2)$$
$$= \int_0^{x_0} \mathrm{d}x\, g_2(x,\, Q^2) - \frac{\tau}{2} F_2(Q^2) G_M(Q^2), \qquad (A15)$$

leading to Eq. (A12b). Thus, splitting into Born and non-Born amplitudes, the BC sum rule constraint is automatically satisfied. In other words, we showed that:

$$\nu S_2^{\text{Born}}(\nu, Q^2)\big|_{\nu \to 0} = \nu \bar{S}_2(\nu, Q^2)\big|_{\nu \to 0} = 0. \qquad (A16)$$

Appendix B: Electron vacuum polarization correction

In this appendix, we consider the one-loop eVP correction to the TPE, shown in Fig. 10. This amounts to multiplying the integrand in Eq. (A7) with $\left[1 - \overline{\Pi}^{(1)}(Q^2)\right]^{-2}$, where the VP is given by:

$$\overline{\Pi}^{(1)}(Q^2) = \Pi^{(1)}(Q^2) - \Pi^{(1)}(0)$$
$$= \frac{\alpha}{3\pi}\Bigg[2\left(1 - \frac{1}{2\tau_e}\right)$$
$$\times\left(\sqrt{1+\frac{1}{\tau_e}}\,\text{arccoth}\,\sqrt{1+\frac{1}{\tau_e}} - 1\right) + \frac{1}{3}\Bigg], \qquad (B1)$$

with $\tau_e = Q^2/4m_e^2$ and m_e the electron mass. The resulting corrections to the polarizability effect are given in Eq. (17).

Appendix C: Theory compilation for hyperfine splitting in μH

In this appendix, we present the details of our theory compilations for the $1S$ and $2S$ hfs in μH, shown in Eqs. (35) and (38). All individual contributions, except the TPE, are listed in Tables 2 and 3. The notation is the same as in Ref. [6]. The difference with Ref. [86] is in the inclusion of ##h10, h14, h18, h19 and h21, as well as some additional radiative corrections to the TPE evaluated in Ref. [13]. Compared to

Table 3 $2S$ hfs in μH. All values in meV

	Contribution	Our Choice	References
h1	Fermi energy, $(Z\alpha)^4$	22.80542	
h2	Breit corr., $(Z\alpha)^6$	0.00258	
h4	μ anomalous magnetic moment corr., $\alpha(Z\alpha)^4$	0.02659	
h5	eVP in 2$^{\text{nd}}$-order PT, $\alpha^2(Z\alpha)^4 m_r$	0.07447	[79, Table 1 b)]
h7	Two-loop corr. to Fermi energy, $\alpha^2(Z\alpha)^4 m_r$	0.00056	[79, Table 2 c) and d)]
h8	One-loop eVP in 1γ int., $\alpha(Z\alpha)^4 m_r$	0.04828	[79, Table 1 a)]
h9	Two-loop eVP in 1γ int., $\alpha^2(Z\alpha)^4 m_r$	0.00037	[79, Table 2 a) and b)]
h10	Further two-loop eVP corr. in 2$^{\text{nd}}$ & 3$^{\text{rd}}$-order PT	0.00037	[79, Table 2 e), f) and g)]
h11	μVP	0.00091	$\sim E_F \alpha(Z\alpha)\, 3/4$
h13	Vertex, $\alpha(Z\alpha)^5$	-0.00311	$\sim E_F \alpha(Z\alpha)\,[\ln 2 - 13/4]$
h14	Higher-order corr. $\alpha(Z\alpha)^6$	-0.00013	[80, Eq. 7.1]
h18	hVP, α^6	0.0006(1)	[84]
h19	Weak interaction contribution	0.00028	[82, Eq. 374]
h21	Higher-order finite-size corr. to Fermi energy	$-0.0022\, r_p^2 + 0.0009$ ≈ -0.00065	[85, Eq. 107]
h28	Recoil corr. with p AMM, α^6	0.00185	[58, Eqs. 1.3 and 2.13]

Refs. [6,84], we suggest to use Eq. (7.1) from Ref. [80]:[13]

$$
E_{nS\text{-hfs}}^{[\alpha(Z\alpha)^6]} = \frac{\alpha(Z\alpha)^2}{\pi} \frac{E_F}{n^3} \left\{ -\frac{8}{3}\ln^2 \frac{2n}{Z\alpha} \right.
$$
$$
+ \left[\frac{37}{36} + \frac{8}{15} + 7(n-1)\right]\ln\frac{n}{2Z\alpha}
$$
$$
+ \left[\frac{22}{3}\ln 2 - \frac{2\pi^2}{9} + 18 - \frac{457}{2700}\right.
$$
$$
\left.\left. - \left(4 + \frac{2993}{8640}\right)(n-1)\right]\right\},
$$

for the higher-order corrections of $\mathcal{O}(\alpha(Z\alpha)^6)$ [#h14]. This includes higher-order muon vacuum polarization corrections. Previously included were only the logarithmically enhanced terms [84]. The effect on the TPE from eVP corrections to the wave function is given in Ref. [87, Eq. (B3)]. For the radius-independent term, we are keeping the error estimate from Ref. [58], which does take into account missing higher-order recoil corrections.

Appendix D: Expansions in terms of polarizabilities

In the following, we will present two further low-energy expansions of the polarizability effect in the hfs. Due to the high-energy asymptotics of the TPE contribution to the hfs, these formulas will merely serve illustrative purposes, while their approximation of the full result is rather poor. Up to

___

[13] Note that some terms in Eqs. (C5) and (C9) of that reference appear to be missing the Fermi energy factor.

and including second moments of the structure functions, Eq. (10) can be written as [62]:

$$
\delta_1 = 2\int_0^\infty \frac{dQ}{Q} \frac{1}{(v_l+1)^2}\left\{ 4(5+4v_l)\,\bar{I}_1(Q^2) - \frac{11+9v_l}{(v_l+1)} \right.
$$
$$
\left. \times \left[\frac{M^2 Q^2}{2\alpha}\gamma_0(Q^2) + \frac{32Z^2 M^6}{Q^6}\int_0^{x_0} dx\, x^4\, g_2(x,Q^2)\right]\right\},
$$
(D1a)

$$
\delta_2 = -24\int_0^\infty \frac{dQ}{Q}\frac{1}{(v_l+1)^2}\left\{\frac{M^2 Q^2}{2\alpha}\left[\delta_{LT}(Q^2) - \gamma_0(Q^2)\right] \right.
$$
$$
\left. - \frac{32Z^2 M^6}{Q^6}\int_0^{x_0} dx\, x^4\, g_2(x,Q^2)\right\},
$$
(D1b)

where $\gamma_0(Q^2)$ and $\delta_{LT}(Q^2)$ are the forward spin and longitudinal-transverse polarizabilities of the proton,

$$
\gamma_0(Q^2) = \frac{16\alpha M^2}{Q^6}\int_0^{x_0} dx\, x^2\left[g_1 - x^2\tau^{-1}g_2\right](x,Q^2)
$$
$$
= \frac{1}{2\pi^2}\int_{v_0}^\infty \frac{dv}{v^3}\sigma_{TT}(v,Q^2),
$$
(D2a)

$$
\delta_{LT}(Q^2) = \frac{16Z^2\alpha M^2}{Q^6}\int_0^{x_0} dx\, x^2\left[g_1 + g_2\right](x,Q^2)
$$
$$
= \frac{1}{2\pi^2}\int_{v_0}^\infty \frac{dv}{Qv^2}\sigma_{LT}(v,Q^2).
$$
(D2b)

The first term in this expansion, corresponds to the $\bar{S}_1(0,Q^2)$ subtraction term already discussed in Sect. 4.3.

Analogously to Ref. [27, Eq. (12)], we try to find an approximation for the hfs master formula assuming that the photon energy in the atomic system is small compared to all other scales. Thus, we expand the numerator of Eq. (A7) around $v = 0$. The resulting approximate formula for the
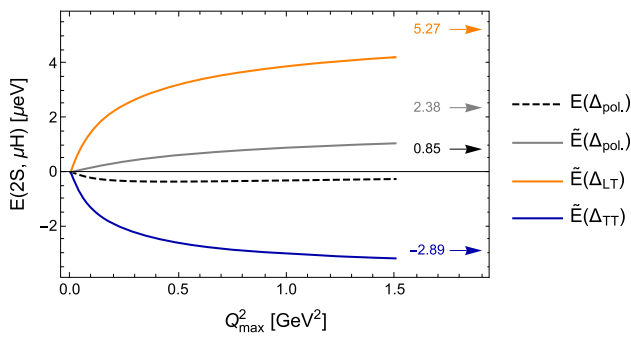
Fig. 11 Polarizability effect on the 2S hyperfine splitting in μH: Comparison of exact result (10) (black dashed line) and approximate formula (D3) (gray solid line)

polarizability contribution to the hfs we call $\tilde{E}$:

$$\tilde{E}(nS) = \frac{E_\text{F}}{n^3} \frac{4\alpha}{\pi m M} \frac{1}{1+\kappa} \int_0^\infty dQ \, Q \, (v_l - 1) \, \bar{I}_1(Q^2). \tag{D3}$$

For BχPT, it gives:

$$\tilde{E}(1S, \text{H}) = 3.0 \, \text{peV}, \tag{D4a}$$

$$\tilde{E}(1S, \mu\text{H}) = 19.0 \, \mu\text{eV}. \tag{D4b}$$

In Fig. 11, we show Eq. (D3) as a running integral with cutoff Q_max (gray line), this time for the 2S hfs in μH. In addition, we show the contributions of the longitudinal-transverse (orange line) and helicity-difference (blue line) cross sections to Eq. (D3), and the exact result from Eq. (10). One can easily see that the quality of the approximation is indeed rather poor.

References

1. R. Pohl et al., The size of the proton. Nature **466**, 213–216 (2010). https://doi.org/10.1038/nature09250
2. R. Pohl et al. (CREMA), Laser spectroscopy of muonic deuterium. Science **353**, 669–673 (2016). https://doi.org/10.1126/science.aaf2468
3. J.J. Krauth et al., Measuring the α-particle charge radius with muonic helium-4 ions. Nature **589**, 527–531 (2021). https://doi.org/10.1038/s41586-021-03183-1
4. A. Antognini et al., Muonic-atom spectroscopy and impact on nuclear structure and precision QED theory. (2022). arXiv:2210.16929 [nucl-th]
5. A. Antognini, F. Nez, K. Schuhmann, F.D. Amaro et al., Proton structure from the measurement of 2S − 2P transition frequencies of muonic hydrogen. Science **339**, 417–420 (2013). https://doi.org/10.1126/science.1230016
6. A. Antognini, F. Kottmann, F. Biraben, P. Indelicato et al., Theory of the 2S−2P Lamb shift and 2S hyperfine splitting in muonic hydrogen. Ann. Phys. **331**, 127–145 (2013). https://doi.org/10.1016/j.aop.2012.12.003. arXiv:1208.2637 [physics.atom-ph]
7. C.E. Carlson, V. Nazaryan, K. Griffioen, Proton structure corrections to hyperfine splitting in muonic hydrogen. Phys. Rev. A

8. **83**, 042509 (2011). https://doi.org/10.1103/PhysRevA.83.042509. arXiv:1101.3239 [physics.atom-ph]
8. P. Amaro et al., Laser excitation of the 1s-hyperfine transition in muonic hydrogen. SciPost Phys. **13**, 020 (2022). https://doi.org/10.21468/SciPostPhys.13.2.020. arXiv:2112.00138 [physics.atom-ph]
9. C. Pizzolotto et al., Measurement of the muon transfer rate from muonic hydrogen to oxygen in the range 70–336 K. Phys. Lett. A **403**, 127401 (2021). https://doi.org/10.1016/j.physleta.2021.127401. arXiv:2105.06701 [physics.atom-ph]
10. C. Pizzolotto et al., The FAMU experiment: muonic hydrogen high precision spectroscopy studies. Eur. Phys. J. A **56**, 185 (2020). https://doi.org/10.1140/epja/s10050-020-00195-9
11. M. Sato et al., Laser spectroscopy of the hyperfine splitting energy in the ground state of muonic hydrogen, in *Proceedings, 20th International Conference on Particles and Nuclei (PANIC 14), Hamburg, Germany, August 24–29, 2014* (2014). https://doi.org/10.3204/DESY-PROC-2014-04/67
12. R. Pohl et al., Laser spectroscopy of muonic atoms and ions, in *Proceedings, 12th International Conference on Low Energy Antiproton Physics (LEAP2016), Kanazawa, Japan, March 6–11, 2016* (2016). http://inspirehep.net/record/1486301/files/516b494d-6503-4a80-abe6-296d75d3e7a8-1609.03440.pdf. arXiv:1609.03440 [physics.atom-ph]
13. A. Antognini, F. Hagelstein, V. Pascalutsa, The proton structure in and out of muonic hydrogen. Annu. Rev. Nucl. Part. Sci. **72**, 389–418 (2022). https://doi.org/10.1146/annurev-nucl-101920-024709. arXiv:2205.10076 [nucl-th]
14. C.E. Carlson, V. Nazaryan, K. Griffioen, Proton structure corrections to electronic and muonic hydrogen hyperfine splitting. Phys. Rev. A **78**, 022517 (2008). https://doi.org/10.1103/PhysRevA.78.022517. arXiv:0805.2603 [physics.atom-ph]
15. R.N. Faustov, I.V. Gorbacheva, A.P. Martynenko, Proton polarizability effect in the hyperfine splitting of the hydrogen atom. Proc. SPIE Int. Soc. Opt. Eng. **6165**, 0M (2006). https://doi.org/10.1117/12.696903. arXiv:hep-ph/0610332
16. O. Tomalak, Two-photon exchange correction to the lamb shift and hyperfine splitting of S levels. Eur. Phys. J. A **55**, 64 (2019). https://doi.org/10.1140/epja/i2019-12743-1. arXiv:1808.09204 [hep-ph]
17. J.P. Chen, Highlights and perspectives of the JLab spin physics program, advanced studies institute on symmetries and spin (SPIN-Praha-2007) Prague, Czech Republic, July 8–14, 2007. Eur. Phys. J. ST **162**, 103–116 (2008). https://doi.org/10.1140/epjst/e2008-00782-y. arXiv:0804.4486 [nucl-ex]
18. K.P. Adhikari et al. (CLAS), Measurement of the Q^2 dependence of the deuteron spin structure function g_1 and its moments at low Q^2 with CLAS. Phys. Rev. Lett. **120**, 062501 (2018). https://doi.org/10.1103/PhysRevLett.120.062501. arXiv:1711.01974 [nucl-ex]
19. X. Zheng et al. (CLAS), Measurement of the proton spin structure at long distances. Nat. Phys. **17**, 736–741 (2021). https://doi.org/10.1038/s41567-021-01198-z. arXiv:2102.02658 [nucl-ex]
20. V. Sulkosky et al. (Jefferson Lab E97-110), Measurement of the ^{3}He spin-structure functions and of neutron (^{3}He) spin-dependent sum rules at $0.035 \leq Q^2 \leq 0.24$ GeV^2. Phys. Lett. B **805**, 135428 (2020). https://doi.org/10.1016/j.physletb.2020.135428. arXiv:1908.05709 [nucl-ex]
21. V. Sulkosky et al. (E97-110), Puzzle with the precession of the neutron spin. Nat. Phys. **17**, 687–692 (2021) [Erratum: Nature Phys. 18, (2022)]. https://doi.org/10.1038/s41567-021-01245-9. arXiv:2103.03333 [nucl-ex]
22. R. Zielinski, The g2p experiment: a measurement of the proton's spin structure functions, Ph.D. thesis, New Hampshire U. (2017). arXiv:1708.08297 [nucl-ex]. http://inspirehep.net/record/1620254/files/arXiv:1708.08297.pdf

23. D. Ruth et al. (Jefferson Lab Hall A g2p), The proton spin structure function g_2 and generalized polarizabilities in the strong QCD regime. (2022). arXiv:2204.10224 [nucl-ex]

24. S. Weinberg, Phenomenological Lagrangians, Physica A **96**, 327 (1979). https://doi.org/10.1016/0378-4371(79)90223-1

25. J. Gasser, H. Leutwyler, Chiral perturbation theory to one loop. Ann. Phys. **158**, 142 (1984). https://doi.org/10.1016/0003-4916(84)90242-2

26. J. Gasser, M.E. Sainio, A. Švarc, Nucleons with chiral loops. Nucl. Phys. B **307**, 779 (1988). https://doi.org/10.1016/0550-3213(88)90108-3

27. J.M. Alarcón, V. Lensky, V. Pascalutsa, Chiral perturbation theory of muonic hydrogen Lamb shift: polarizability contribution. Eur. Phys. J. C **74**, 2852 (2014). https://doi.org/10.1140/epjc/s10052-014-2852-0. arXiv:1312.1219 [hep-ph]

28. J. Gegelia, G. Japaridze, X.Q. Wang, Is heavy baryon approach necessary? J. Phys. G **29**, 2303–2309 (2003). https://doi.org/10.1088/0954-3899/29/9/322. arXiv:hep-ph/9910260

29. T. Fuchs, J. Gegelia, G. Japaridze, S. Scherer, Renormalization of relativistic baryon chiral perturbation theory and power counting. Phys. Rev. D **68**, 056005 (2003). https://doi.org/10.1103/PhysRevD.68.056005. arXiv:hep-ph/0302117

30. V. Pascalutsa, M. Vanderhaeghen, S.N. Yang, Electromagnetic excitation of the $\Delta(1232)$-resonance. Phys. Rep. **437**, 125–232 (2007). https://doi.org/10.1016/j.physrep.2006.09.006. arXiv:hep-ph/0609004

31. L. Geng, Recent developments in SU(3) covariant baryon chiral perturbation theory. Front. Phys. China **8**, 328–348 (2013). https://doi.org/10.1007/s11467-013-0327-7. arXiv:1301.6815 [nucl-th]

32. K. Pachucki, Theory of the lamb shift in muonic hydrogen. Phys. Rev. A **53**, 2092–2100 (1996). https://doi.org/10.1103/PhysRevA.53.2092

33. A. Antognini, Y.-H. Lin, and U.-G. Meißner, Precision calculation of the recoil–finite-size correction for the hyperfine splitting in muonic and electronic hydrogen. Phys. Lett. B **835**, 137575 (2022). https://doi.org/10.1016/j.physletb.2022.137575 arXiv:2208.04025 [nucl-th]

34. F. Hagelstein, V. Pascalutsa, The subtraction contribution to the muonic-hydrogen lamb shift: a point for lattice QCD calculations of the polarizability effect. Nucl. Phys. A **1016**, 122323 (2021). https://doi.org/10.1016/j.nuclphysa.2021.122323. arXiv:2010.11898 [hep-ph]

35. V. Biloshytskyi, I. Ciobotaru-Hriscu, F. Hagelstein, V. Lensky, V. Pascalutsa, The QED of Bernabéu–Tarrach sumrule for electric polarizability and its implication for the Lamb shift. (2023). arXiv:2305.08814 [hep-ph]

36. F. Hagelstein, R. Miskimen, V. Pascalutsa, Nucleon Polarizabilities: from Compton scattering to hydrogen atom. Prog. Part. Nucl. Phys. **88**, 29–97 (2016). https://doi.org/10.1016/j.ppnp.2015.12.001. arXiv:1512.03765 [nucl-th]

37. V. Nazaryan, C.E. Carlson, K.A. Griffioen, New experimental constraints on polarizability corrections to hydrogen hyperfine structure. Phys. Rev. Lett. **96**, 163001 (2006). https://doi.org/10.1103/PhysRevLett.96.163001. arXiv:hep-ph/0512108

38. V. Lensky, V. Pascalutsa, Predictive powers of chiral perturbation theory in Compton scattering off protons. Eur. Phys. J. C **65**, 195–209 (2010). https://doi.org/10.1140/epjc/s10052-009-1183-z

39. C. Patrignani et al (Particle Data Group), Review of particle physics. Chin. Phys. C **40**, 100001 (2016). https://doi.org/10.1088/1674-1137/40/10/100001

40. V. Lensky, J.M. Alarcón, V. Pascalutsa, Moments of nucleon structure functions at next-to-leading order in baryon chiral perturbation theory. Phys. Rev. C **90**, 055202 (2014). https://doi.org/10.1103/PhysRevC.90.055202. arXiv:1407.2574 [hep-ph]

41. J. M. Alarcón, F. Hagelstein, V. Lensky, V. Pascalutsa, Forward doubly-virtual Compton scattering off the nucleon in chiral perturbation theory: the subtraction function and moments of unpolarized structure functions. Phys. Rev. D **102**, 014006 (2020). https://doi.org/10.1103/PhysRevD.102.014006. arXiv:2005.09518 [hep-ph]

42. J.M. Alarcón, F. Hagelstein, V. Lensky, V. Pascalutsa, Forward doubly-virtual Compton scattering off the nucleon in chiral perturbation theory: II. Spin polarizabilities and moments of polarized structure functions. Phys. Rev. D **102**, 114026 (2020). https://doi.org/10.1103/PhysRevD.102.114026. arXiv:2006.08626 [hep-ph]

43. V. Pascalutsa, D.R. Phillips, Effective theory of the $\Delta(1232)$ in Compton scattering off the nucleon. Phys. Rev. C **67**, 055202 (2003). https://doi.org/10.1103/PhysRevC.67.055202. arXiv:nucl-th/0212024

44. V. Bernard, T.R. Hemmert, U.-G. Meissner, Spin structure of the nucleon at low-energies. Phys. Rev. D **67**, 076008 (2003). https://doi.org/10.1103/PhysRevD.67.076008. arXiv:hep-ph/0212033

45. V. Bernard, Chiral perturbation theory and baryon properties. Prog. Part. Nucl. Phys. **60**, 82–160 (2008). https://doi.org/10.1016/j.ppnp.2007.07.001

46. V. Bernard, E. Epelbaum, H. Krebs, U.G. Meißner, New insights into the spin structure of the nucleon. Phys. Rev. D **87**, 054032 (2013). https://doi.org/10.1103/PhysRevD.87.054032. arXiv:1209.25231 [hep-ph]

47. T.R. Hemmert, B.R. Holstein, J. Kambor, Systematic $1/M$ expansion for spin 3/2 particles in baryon chiral perturbation theory. Phys. Lett. B **395**, 89–95 (1997). https://doi.org/10.1016/S0370-2693(97)00049-X. arXiv:hep-ph/9606456

48. X.-D. Ji, J. Osborne, Generalized sum rules for spin dependent structure functions of the nucleon. J. Phys. G **27**, 127 (2001). https://doi.org/10.1088/0954-3899/27/1/308. arXiv:hep-ph/9905410

49. K.B. Vijaya Kumar, J.A. McGovern, M.C. Birse, Spin polarisabilities of the nucleon at NLO in the chiral expansion. Phys. Lett. B **479**, 167–172 (2000). https://doi.org/10.1016/S0370-2693(00)00340-3. arXiv:hep-ph/0002133

50. T.R. Hemmert, B.R. Holstein, G. Knochlein, S. Scherer, Virtual Compton scattering off the nucleon in chiral perturbation theory. Phys. Rev. D **55**, 2630–2643 (1997). https://doi.org/10.1103/PhysRevD.55.2630. arXiv:nucl-th/9608042

51. T.R. Hemmert, B.R. Holstein, G. Knochlein, S. Scherer, Generalized polarizabilities and the chiral structure of the nucleon. Phys. Rev. Lett. **79**, 22–25 (1997). https://doi.org/10.1103/PhysRevLett.79.22. arXiv:nucl-th/9705025

52. T.R. Hemmert, B.R. Holstein, G. Knochlein, D. Drechsel, Generalized polarizabilities of the nucleon in chiral effective theories. Phys. Rev. D **62**, 014013 (2000). https://doi.org/10.1103/PhysRevD.62.014013. arXiv:nucl-th/9910036

53. C.W. Kao, M. Vanderhaeghen, Generalized spin polarizabilities of the nucleon in heavy baryon chiral perturbation theory at next-to-leading order. Phys. Rev. Lett. **89**, 272002 (2002). https://doi.org/10.1103/PhysRevLett.89.272002. arXiv:hep-ph/0209336

54. C.-W. Kao, B. Pasquini, M. Vanderhaeghen, New predictions for generalized spin polarizabilities from heavy baryon chiral perturbation theory. Phys. Rev. D **70**, 114004 (2004). https://doi.org/10.1103/PhysRevD.92.119906 [Erratum: Phys. Rev. D 92, no. 11, 119906 (2015)]. https://doi.org/10.1103/PhysRevD.70.114004. arXiv:hep-ph/0408095

55. V. Lensky, V. Pascalutsa, M. Vanderhaeghen, C. Kao, Spin-dependent sum rules connecting real and virtual Compton scattering verified. Phys. Rev. D **95**, 074001 (2017). https://doi.org/10.1103/PhysRevD.95.074001. arXiv:1701.01947 [hep-ph]

56. A. Pineda, Leading chiral logarithms to the hyperfine splitting of the hydrogen and muonic hydrogen. Phys. Rev. C **67**, 025201 (2003). https://doi.org/10.1103/PhysRevC.67.025201. arXiv:hep-ph/0210210

57. C. Peset, A. Pineda, The two-photon exchange contribution to muonic hydrogen from chiral perturbation theory. Nucl. Phys. B

887, 69–111 (2014). https://doi.org/10.1016/j.nuclphysb.2014.07.027. arXiv:1406.4524 [hep-ph]

58. C. Peset, A. Pineda, Model-independent determination of the two-photon exchange contribution to hyperfine splitting in muonic hydrogen. JHEP **04**, 060 (2017). https://doi.org/10.1007/JHEP04(2017)060. arXiv:1612.05206 [nucl-th]

59. A. Pineda, Learning about the chiral structure of the proton from the hyperfine splitting, in *17th International IUPAP Conference on Few-Body Problems in Physics* (2003). arXiv:hep-ph/0308193

60. C. Peset, A. Pineda, Model-independent determination of the Lamb shift in muonic hydrogen and the proton radius. Eur. Phys. J. A **51**, 32 (2015). https://doi.org/10.1140/epja/i2015-15032-1. arXiv:1403.3408 [hep-ph]

61. F. Hagelstein, $\Delta(1232)$-resonance in the hydrogen spectrum, in *Proceedings, 11th International Workshop on the Physics of Excited Nucleons (NSTAR 2017): Columbia, SC, USA, August 20-23, 2017, Few Body Systems*, vol. **59** (2018), p. 93. https://doi.org/10.1007/s00601-018-1403-x. arXiv:1801.09790 [nucl-th]

62. F. Hagelstein, Exciting nucleons in Compton scattering and hydrogen-like atoms. Ph.D. thesis, JGU Mainz (2017). https://doi.org/10.13140/RG.2.2.25062.73281. arXiv:1710.00874 [nucl-th]

63. Y. Prok et al. (CLAS), Moments of the spin structure functions g_1^p and g_1^d for $0.05 < Q^2 < 3.0 \mathrm{GeV}^2$. Phys. Lett. B **672**, 12–16 (2009). https://doi.org/10.1016/j.physletb.2008.12.063. arXiv:0802.2232 [nucl-ex]

64. K.V. Dharmawardane et al. (CLAS), Measurement the x- and Q^2-dependence of the asymmetry A_1 on the nucleon. Phys. Lett. B **641**, 11–17 (2006). https://doi.org/10.1016/j.physletb.2006.08.011. arXiv:nucl-ex/0605028

65. H. Hellwig, R.F.C. Vessot, M.W. Levine, P.W. Zitzewitz, D.W. Allan, D.J. Glaze, Measurement of the unperturbed hydrogen hyperfine transition frequency. IEEE Trans. Instrum. Meas. **19**, 200–209 (1970). https://doi.org/10.1109/TIM.1970.4313902

66. S.G. Karshenboim, Some possibilities for laboratory searches for variations of fundamental constants. Can. J. Phys. **78**, 639–678 (2000). https://doi.org/10.1139/cjp-78-7-639. arXiv:physics/0008051

67. O. Tomalak, Hyperfine splitting in ordinary and muonic hydrogen. Eur. Phys. J. A **54**, 3 (2018). https://doi.org/10.1140/epja/i2018-12453-2. arXiv:1709.06544 [hep-ph]

68. Y.-H. Lin, H.-W. Hammer, U.-G. Meißner, New insights into the nucleon's electromagnetic structure. Phys. Rev. Lett. **128**, 052002 (2022). https://doi.org/10.1103/PhysRevLett.128.052002. arXiv:2109.12961 [hep-ph]

69. K. Borah, R.J. Hill, G. Lee, O. Tomalak, Parametrization and applications of the low-Q^2 nucleon vector form factors. Phys. Rev. D **102**, 074012 (2020). https://doi.org/10.1103/PhysRevD.102.074012. arXiv:2003.13640 [hep-ph]

70. M.O. Distler, J.C. Bernauer, T. Walcher, The RMS charge radius of the proton and Zemach moments. Phys. Lett. B **696**, 343–347 (2011). https://doi.org/10.1016/j.physletb.2010.12.067. arXiv:1011.1861 [nucl-th]

71. J.J. Kelly, Simple parametrization of nucleon form factors. Phys. Rev. C **70**, 068202 (2004). https://doi.org/10.1103/PhysRevC.70.068202

72. R. Bradford, A. Bodek, H. S. Budd, J. Arrington, A new parameterization of the nucleon elastic form-factors, in *NuInt05, proceedings of the 4th International Workshop on Neutrino-Nucleus Interactions in the Few-GeV Region, Okayama, Japan, 26–29 September 2005*. Nucl. Phys. Proc. Suppl. **159**, 127–132 (2006). https://doi.org/10.1016/j.nuclphysbps.2006.08.028. arXiv:hep-ex/0602017

73. J. Arrington, W. Melnitchouk, J.A. Tjon, Global analysis of proton elastic form factor data with two-photon exchange corrections. Phys. Rev. C **76**, 035205 (2007). https://doi.org/10.1103/PhysRevC.76.035205. arXiv:0707.1861 [nucl-ex]

74. J. Arrington, I. Sick, Precise determination of low-Q nucleon electromagnetic form factors and their impact on parity-violating e-p elastic scattering. Phys. Rev. C **76**, 035201 (2007). https://doi.org/10.1103/PhysRevC.76.035201. arXiv:nucl-th/0612079

75. A.V. Volotka, V.M. Shabaev, G. Plunien, G. Soff, Zemach and magnetic radius of the proton from the hyperfine splitting in hydrogen. Eur. Phys. J. D **33**, 23–27 (2005). https://doi.org/10.1140/epjd/e2005-00025-9. arXiv:physics/0405118

76. H.A. Bethe, E.E. Salpeter, *Quantum Mechanics of One- and Two-Electron Atoms* (Springer, Berlin, 1957)

77. D. Drechsel, B. Pasquini, M. Vanderhaeghen, Dispersion relations in real and virtual Compton scattering. Phys. Rep. **378**, 99–205 (2003). https://doi.org/10.1016/S0370-1573(02)00636-1. arXiv:hep-ph/0212124

78. H. Burkhardt, W.N. Cottingham, Sum rules for forward virtual Compton scattering. Ann. Phys. **56**, 453–463 (1970). https://doi.org/10.1016/0003-4916(70)90025-4

79. S.G. Karshenboim, E.Y. Korzinin, V.G. Ivanov, Hyperfine splitting in muonic hydrogen: QED corrections of the $\alpha 2$ order. JETP Lett. **89**, 216–216 (2009). https://doi.org/10.1134/S0021364009040110

80. S.J. Brodsky, G.W. Erickson, Radiative level shifts. 3. Hyperfine structure in hydrogenic Atoms. Phys. Rev. **148**, 26–46 (1966). https://doi.org/10.1103/PhysRev.148.26

81. R.N. Faustov, A.P. Martynenko, Contribution of hadronic vacuum polarization to hyperfine splitting of muonic hydrogen. Phys. At. Nucl. **61**, 471–475 (1998). arXiv:hep-ph/9709374

82. M.I. Eides, H. Grotch, V.A. Shelyuto, Theory of light hydrogen-like atoms. Phys. Rep **342**, 63–261 (2001). https://doi.org/10.1016/S0370-1573(00)00077-6. arXiv:hep-ph/0002158

83. G.T. Bodwin, D.R. Yennie, Some recoil corrections to the hydrogen hyperfine splitting. Phys. Rev. D **37**, 498 (1988). https://doi.org/10.1103/PhysRevD.37.498

84. E. Borie, Lamb shift in light muonic atoms: revisited. Ann. Phys. **327**, 733–763 (2012). https://doi.org/10.1016/j.aop.2011.11.017. arXiv:1103.1772 [physics.atom-ph]

85. P. Indelicato, Nonperturbative evaluation of some QED contributions to the muonic hydrogen $n = 2$ Lamb shift and hyperfine structure. Phys. Rev. A **87**, 022501 (2013). https://doi.org/10.1103/PhysRevA.87.022501. arXiv:1210.5828 [physics.atom-ph]

86. C. Peset, A. Pineda, O. Tomalak, The proton radius (puzzle?) and its relatives. Prog. Part. Nucl. Phys. **121**, 103901 (2021). https://doi.org/10.1016/j.ppnp.2021.103901. arXiv:2106.00695 [hep-ph]

87. S.G. Karshenboim, V.A. Shelyuto, Hadronic vacuum-polarization contribution to various QED observables. Eur. Phys. J. D **75**, 49 (2021). https://doi.org/10.1140/epjd/s10053-021-00052-4